EFFECT OF TEMPERATURE DEPENDENT VISCOSITY ON MIXED CONVECTION HEAT TRANSFER IN AN UNCONFINED FLOW ACROSS A CIRCULAR CYLINDER

A DISSERTATION

Submitted in partial fulfillment of the requirements for the award of the degree of

INTEGRATED DUAL DEGREE

(Bachelor of Technology & Master of Technology)

in

CHEMICAL ENGINEERING

(With Specialization in Hydrocarbon Engineering)

By

KAKKAR PRATIK DILIPKUMAR

DEPARTMENT OF CHEMICAL ENGINEERING
INDIAN INSTITUTE OF TECHNOLOGY ROORKEE
ROORKEE -247 667 (INDIA)

JUNE, 2012

Candidate's Declaration

I hereby declare that the work presented in this report entitled **"Effect of temperature dependent viscosity on Mixed Convection in an unconfined flow across a circular cylinder"** submitted in partial fulfilment of the requirements for the award of Integrated Dual Degree in Chemical Engineering with specialisation in Hydrocarbon Engineering, Indian Institute of Technology Roorkee, is an authentic record of my original work carried out under the guidance of **Dr. Ram Prakash Bharti**, Assistant Professor, Department of Chemical Engineering, Indian Institute of Technology Roorkee.

I have not submitted the matter embodied in this Report for the award of any other degree.

Pratik

Date: 07-06-2012 Kakkar Pratik Dilipkumar

Place: Roorkee Enrollment No. 071105

Certificate

This is to certify that the above statement made by the candidate is correct to the best of my knowledge and belief.

07/06/12

Dr.Ram Prakash Bharti

Assistant Professor

Department of Chemical Engineering

IIT Roorkee

CONTENTS

List of Figures

LIST OF TABLES

NOMENCLATURE

C_D Total drag coefficient, dimensionless

C_{DF} Frictional component of the drag coefficient, dimensionless

C_{DP} Pressure component of the drag coefficient, dimensionless

D Diameter of the cylinder, m

Gr Grashof number, dimensionless

h Local convective heat transfer coefficient, W/(m2 K)

k Thermal conductivity of the fluid, W/(m K)

n power-law flow behavior index, dimensionless

Nu surface averaged Nusselt number, dimensionless

Nu (θ) Local Nusselt number over the surface of the cylinder, dimensionless

P pressure, Pa

Pr Prandtl number, dimensionless

Re Reynolds number, dimensionless

Ri Richardson number () *Gr/Re*2), dimensionless.

T Temperature, K

T_0 Temperature of the fluid at the inlet,

T_w Temperature of the surface of the cylinder, K

U_0 Uniform inlet velocity of the fluid, m/s

U_x, U_y *x*- and *y*-components of the velocity, m/s

(x, y) Transverse and stream wise coordinates, m

B Temperature thinning index

Greek Symbols

η viscosity, Pa s

θ Angular displacement from the front stagnation (θ) 0), deg

ω Vorticity, dimensionless.

ρ Density of the fluid, kg/m3

τ extra stress tensor, Pa

CHAPTER - 1

INTRODUCTION

1.1 Motivation

Newtonian or non-Newtonian fluid flow across circular cylinder has been studied extensively because of its numerous practical applications Bluff body has received a great deal of attention especially for the prediction of loads on engineering structures such as offshore platform supports, ocean pipelines, high buildings, bridge piers etc. and for analysis of wake control in aeronautical engineering as well (Mohammed and Salman, 2007). Reliable knowledge of flow characteristics and hydrodynamic forces exerted on bodies immersed in fluids is needed to design the support structures exposed to non-Newtonian fluids in polymer melt operations. Due to the simple nature of the geometry, this flow has been frequently used to gain insights into the physics of flow and to understand the wake dynamics of bluff bodies. Moreover, this geometry has also been used to validate numerical solution methodologies and to assess the efficiency of various numerical algorithms.

Over the past few decades, considerable attention has been given to this geometric configuration and a voluminous body of knowledge incorporating wide ranging phenomena has emerged. Several excellent reviews and even entire books devoted to this geometric configuration have appeared in literature (e.g., see Ghosh et al., 1994; Ahmad, 1996; Zdravkovich, 1997, 2003, etc.).

This simple flow configuration displays wide variety of flow phenomena depending on various factors like nature of approaching flow (laminar, turbulent; non-uniform, uniform), cross section of body (circular or non-circular), fluid behaviour (Newtonian or non-Newtonian), flow configuration (confined or unconfined), number of obstacles and their arrangement (inline or staggered), the range of kinematic parameters (Reynolds number, Prandtl number, Richardson number), etc. In addition to this, the rate of heat

transfer from cylinder to streaming fluid is influenced by the type of boundary layer prescribed at the wall of the cylinder, namely, constant wall temperature (CWT) or uniform heat flux (UHF).

It is well known that many materials exhibit a range of non-Newtonian flow characteristics. For example, substances having high molecular weight (natural and synthetic polymers, gums) soap solutions and multiphase mixtures (foams, emulsions & suspensions) exhibit a wide range of rheological complexities including shear dependent viscosity, viscoelasticity & yield stress, etc.

1.2.1 Newtonian Fluids

A Newtonian fluid is a fluid whose stress versus strain rate curve is linear and passes through the origin. The slope of the curve is called the Newtonian viscosity, is independent of shear rate or shear stress at a given temperature and pressure. Some examples are air and other gases, water and most substances having low molecular weights, organic liquids, etc.

1.2.2 Non-Newtonian Fluids

A non-Newtonian fluid is a fluid whose flow properties differ in any way from those of Newtonian fluids. In other words, at a given temperature and pressure, slope of the shear stress versus shear strain curve is not constant, i.e., the viscosity is dependent on shear rate or shear stress and sometime on the kinematic history of the fluid which is under consideration. A detailed literature on the non-Newtonian fluids and their classification can be found in various texts (Carreau et al., 1997; Chhabra and Richardson, 1999; Gupta, 2005).

1.3 Time-Independent Fluids

Many fluids do not follow the Newton's law of viscosity, but is a function of shear rate only. Such fluids are called as 'time independent' or 'purely viscous' or 'inelastic' fluids. On the basis of the stress versus strain curve these can be further divided into following classes (Figure 1.1(a)):

(a) *Shear – thinning or pseudo plastic:* In these types of fluids apparent viscosity decreases with shear rate and the flow curve is concave downward. The extent of pseudo plasticity increases as slope decreases. Most high molecular weight polymeric systems (solutions, melts, blends) and multiphase mixtures (solutions, melts, blends, etc.) exhibit shear thinning characteristics.

(b) *Shear – thickening or dilatant:* In these types of fluids apparent viscosity increases with shear rate and the flow curve is concave upward. Very few fluids such as corn flour in water, kaolin in water, suspensions of beach sand, etc. display this kind of behaviour.

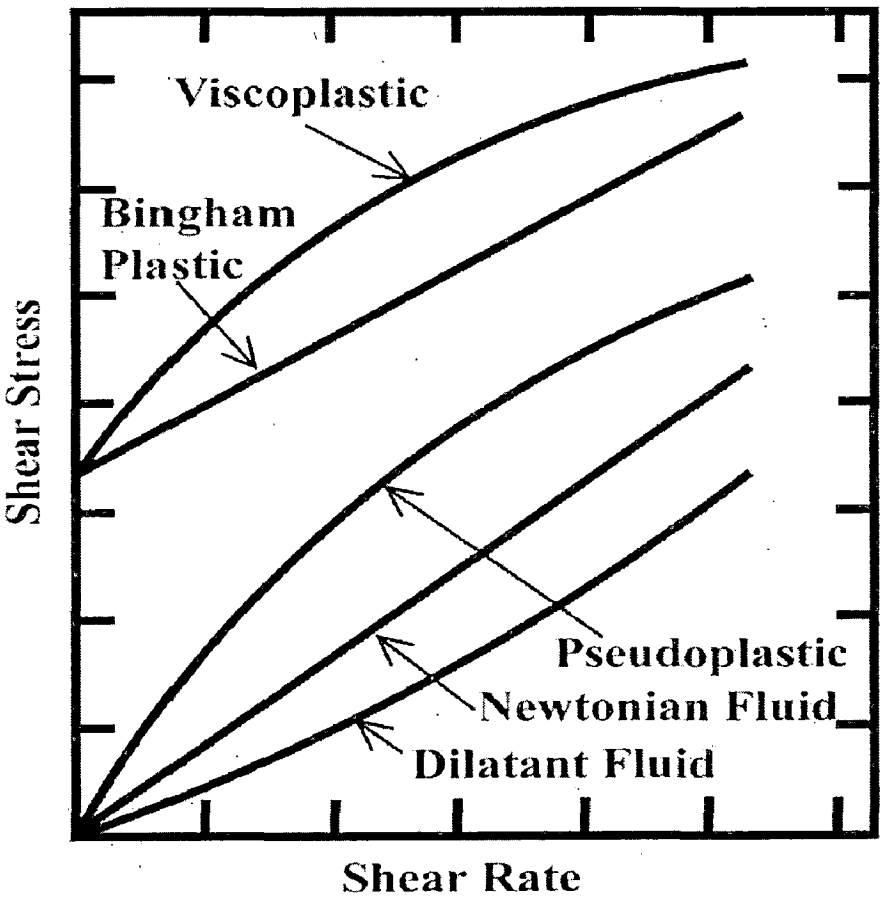

Figure 1 Rheogram for non-Newtonian fluids (Chhabra and Richardson, 1999; Chhabra, 2006)

(c) *Viscoplastic fluids:* These fluids are characterized by the existence of a minimum stress which must be exceeded before fluid starts to

deform. Once this stress exceeds the yield stress, the flow curve may be linear or non-linear, but it will not pass through origin. This type of fluid shows creeps and behaves like a soft elastic solid whereas once the shear stress exceeds the yield stress it behaves like a fluid. Examples of viscoplastic fluids include chocolates, meat extract, carbopol solutions, paints, foams, etc.

1.4 Computational Fluid Dynamics

Computers along with the advanced mathematical techniques has opened a relatively new and powerful field of aerodynamics called Computational Fluid Dynamics (CFD). In its simplest terms, CFD is the process of taking a physical flow problem, breaking it down into a suitable set of equations, and solving them on a digital computer. (Arvel Gentry et al. 1998).

Computational fluid dynamics (CFD) is the science of predicting fluid flow, heat and mass transfer, chemical reactions, and related phenomenon by solving numerically the set of governing mathematical equations. CFD embraces a variety of technologies including mathematics, computer science, engineering and physics and these disciplines have to be brought together to provide the means of modelling fluid flow.

CFD approaches the set of partial differential equations describing the fundamental laws of motion. The fundamental basis of CFD problem is the Navier-stokes equations which define any single fluid flow. These equations can be solved by removing terms describing vorticity, then on linearizing these equations and solved by a CFD solver code.

1.5 Meshing

GAMBIT 2.3.16: A geometric modelling and grid generation tool often included with FLUENT technology. GAMBIT software allows users to create their own geometry or import geometry from most CAD packages. It can automatically mesh surfaces and volumes while allowing the user to control the mesh through the use of sizing function and boundary layer meshing.

The partial differential equations that govern fluid flow and heat transfer are not usually amenable to analytical solution, except for very simple cases. Therefore, in order to analyse fluid flows, domains are splits into smaller sub domains. The governing equations are then discretized and solved inside each of these formed sub domains. Typically, one of three below mentioned methods is used to solve the approximate version of the system of equations: finite volume, finite elements, or finite differences. The sub domains are often called a mesh or grid.

Due to the recent developments in CFD, better algorithms and more computational power have become available to CFD analysis, resulting in diverse solution techniques.

1.6 Organization of Dissertation

The entire dissertation has been divided into various chapters. Different types of fluids are studied in Chapter 1. Chapter 2 deals with the previous work that has been done to study the momentum and heat transfer characteristics of flow around cylinder. In Chapter 3, the problem statement is formed and governing equations are presented with boundary conditions along with solution methodology. Development of model using GAMBIT and further solution procedure in FLUENT has also been discussed. In Chapter 4, the model has been validated with the results given in literature and then the model developed is used to generate extensive flow and heat transfer data. Finally, conclusions are given in the Chapter 5 along with the recommendations for future study.

CHAPTER – 2

LITERATURE REVIEW

This chapter presents an overview of various aspects including the flow regimes associated with the flow past a circular cylinder, which helps in the basic understanding of the flow phenomena. It is further followed by a brief literature review available for the flow and heat transfer across a cylinder in different configurations.

2.1.1 Bluff Bodies

From the point of view of fluid mechanics bodies can be classified in two kinds: streamlined and bluff bodies. The shape along which streamlines follow a smooth path are called streamlined bodies, e.g., an aerofoil, etc. On the other hand, bodies around which streamlines break away with sharp changes in parameters such as velocity, etc., is called a bluff body. Bluff bodies may also have sharp edges or corners, such as flat plates, triangular, square, rectangular, and polygonal cylinders or may be round like spheres and circular, elliptical and arbitrary oval cylinders. The point of separation is fixed by the sharp edges for the former type whereas it can adjust itself in response to the flow structure for the rounded bluff bodies. A region of separated flow also occurs over a large portion of the surface of bluff body, which results in a high proportion of form or drag and a large wake region. A streamlined body will have lower flow resistance than a bluff body for a given frontal area and velocity. In streamlined bodies, the regions where losses occur are inside the boundary layers and wake that remain reasonably thin, whereas in case of bluff bodies, adverse pressure gradient causes the boundary layers to separate, creating a large wake filled with energetic eddies dissipating a large part of mechanical energy and thereby increasing the drag.

2.1.2 Regions of Disturbed Flow

When there is a relative motion between the fluid and the bluff body (circular cylinder in this context), a region of disturbance is always formed around the body, nature of which depends upon the flow parameters. In spite of some differences in the shape and size of the disturbed region, some similarities have been observed. Disturbed flow can be divided in to four regions on the basis of the ratio of the local velocity (u) to the free stream velocity (u_{max}) as shown in figure 2.

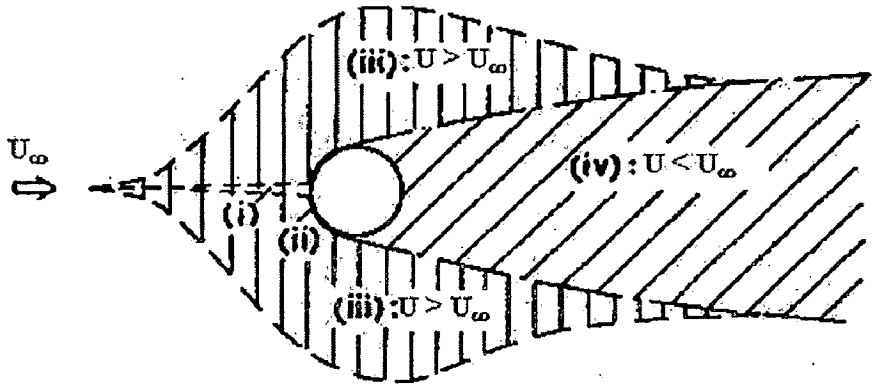

Figure 2 Disturbances regions across cylinder (Zdravkovich, 1997).

(i) Stagnation region: A narrow region of upstream retarded flow. Here $u << u_{max}$

(ii) Boundary layer region: Two boundary layers are attached to the surface of the cylinder.

(iii) Displaced and accelerated flow region: The extent of displaced region is strongly influenced by the confining walls (blockage ratio). Here $u > u_{max}$.

(iv) Wake region: The formation and destruction of flow structures in this region depends upon the state of flow i.e. laminar or turbulent. Here $u < u_{max}$.

It is understood that above a critical Reynolds number, flow around slender cylindrical bodies, in general, exhibits the well-known time periodic vortex shedding as a result of the von-Karman instability leading to alternate vertical structures known as the von Karman vortex street. This phenomenon is responsible for fluctuating forces on the body that may cause structural vibrations, acoustic noise emissions, and sometimes resonance triggering the failure of structures. Thus, it is important from engineering point of view to investigate flow around these bodies.

2.1.3 Governing Parameters

The governing parameters for the flow and heat transfer in non-Newtonian fluids are Reynolds number (Re), Prandtl number or Peclet number (Pe) and power law index (n). Additional parameters emerge for mixed convection such as Richardson number (Ri) and parameter for temperature dependent viscosity (b). The effect of these parameters on Drag Coefficient (C_D) and surface averaged Nusselt number (Nu) is analysed in this study.

2.2 Dimensionless Groups

Various dimensionless groups can be considered to characterize the flow of power law fluids. The simple scaling and dimensional considerations of this flow suggest the following dimensionless numbers to characterise the flow.

Reynolds Number (*Re*)

$$Re = \frac{\rho D^n U_{avg}^{2-n}}{m} \tag{1}$$

where D, ρ and U_{avg} are the diameter of the cylinder, density of the fluid and average inlet velocity of the fluid, respectively.

For an uncontrolled flow, $U_{avg} = U_\infty$ (free stream velocity).

Prandtl Number (*Pr*)

$$Pr = \frac{c_p m}{k}\left(\frac{U_{avg}}{D}\right)^{n-1} \tag{2}$$

where c_p and k are the specific heat and thermal conductivity of the fluid, respectively.

Peclet Number (*Pe*)

$$Pe = Re \times \Pr = \frac{pc_p U_{avg} D}{k} \quad (3)$$

Peclet Number is independent of the power-law constants and thus offers the possibility of reconciling the results for Newtonian and power-law fluids.

Nusselt Number (*Nu*)

$$Nu = \frac{hD}{k} \quad (4)$$

Where, h is the convective heat transfer coefficient.

Grashof Number (*Gr*)

$$Gr = \frac{g\bar{\beta}\Delta T \rho^2 D^3}{m^2}\left(\frac{U_{avg}}{D}\right)^{2(1-n)} \quad (5)$$

where g, $\bar{\beta}$ and ΔT are the coefficient of gravitational force, volumetric thermal expansion coefficient and temperature difference, respectively.

Rayleigh Number (*Ra*)

$$Ra = Gr \times \Pr = \frac{g\bar{\beta}\Delta T D^3 \rho^2 c_p}{k\mu} \quad (6)$$

Both Gr and Ra are inter-related and are relevant when heat transfer occurs by free convection.

Richardson Number (*Ri*)

$$Ri = \frac{Gr}{Re^2} = \frac{g\bar{\beta}\Delta T D}{U_{avg}^2} \quad (7)$$

$Ri = 0$: Forced Convection; $Ri \rightarrow \infty$: free convection

$Ri > 0$: aiding flow mixed convection (heated cylinder i.e., where the buoyancy acts in the same direction as the flow).

$Ri < 0$: opposing flow mixed convection (cooled cylinder i.e., where the buoyancy and the flow are in the opposite direction).

Drag Coefficient (C_D)

$$C_D = \frac{F_D}{\frac{1}{2}\rho U_{max}^2 DL} = \underbrace{\frac{F_{DF}}{\frac{1}{2}\rho U_{max}^2 DL}}_{\text{Viscous Component}} + \underbrace{\frac{F_{DP}}{\frac{1}{2}\rho U_{max}^2 DL}}_{\text{Pressure Component}}$$

where F_D, F_{DF} and F_{DP} are the total, friction and pressure drag forces, respectively. U_{max} is the maximum velocity of the fluid at the inlet (for unconfirmed flow, $U_{max} = U_\infty$) and L is the length of the cylinder.

Lift Coefficient (C_L)

$$C_L = \frac{F_L}{\frac{1}{2}\rho U_{max}^2 DL} = \underbrace{\frac{F_{LF}}{\frac{1}{2}\rho U_{max}^2 DL}}_{\text{Viscous Component}} + \underbrace{\frac{F_{LP}}{\frac{1}{2}\rho U_{max}^2 DL}}_{\text{Pressure Component}}$$

where F_L, F_{LF} and F_{LP} are the total, friction and pressure lift forces, respectively.

2.4 Referred Literature

The bulk of the information on momentum and heat transfer from a cylinder is available for only Newtonian fluids in steady flow regime. Recent studies have evolved with different modifications like detailed hydrodynamics and heat transfer of non-Newtonian power-law fluids across a single and multiple circular cylinder (for instance, see Bharti et al. 2005, 2006, 2007; Patnana et al. 2010; Sivakumar et al. 2006). Recently, vortex dynamics and drag and heat transfer characteristics of power law fluid in unconfined flow configuration has also been studied over a wide range of power law index ($0.4<n<1.8$), Reynolds number ($40<Re<140$) (Patnana et al., 2009, 2010). Besides that, there have been various studies on mixed convection flow across a circular cylinder submerged in power-law medium (for instance Soares et al.,2005; Dhiman et al., 2007; Mohammed and Salman 2007;

Soares et al.,2009; Srinivas et al.,2009). A brief review of the available literature on mixed convection flow across a single circular cylinder is presented below:

Juncu (2004) has analysed the unsteady heat/mass transfer between a circular cylinder and a surrounding fluid flow. Numerical investigations were carried out for the cylinder Re=2 and 20 and different value of the Prandtl/Schmidt numbers. The heat and mass balance equation were solved numerically in cylindrical coordinates by the ADI method. In the range of Reynolds numbers investigated, the laminar flow around a circular cylinder has two regimes: steady flow without separation (Re<5) and steady flow with two symmetric vortices behind the cylinder ($5<Re<Re_{crt}=46$).

Chakraborty et al. (2004) studied numerically the steady flow of an incompressible Newtonian fluid past a circular cylinder confined in a plane rectangular channel using FLUENT 6.3 to carry out two-dimensional steady state analysis for an uniform inlet velocity and for different values of the Reynolds numbers in the range between 0.1 and 200 and blockage ratios in the range between 1.54 and 20. It showed that the drag coefficient, C_D decreased with an increase in Re for a fixed value of λ. It was found that C_D increased with a decrease in λ for a fixed Re due to the fact that the walls exert an extra retardation force on the cylinder. However, the increase in the pressure drag was more significant than that in the friction drag. An expression for drag coefficient as a function of the blockage ratio was developed.

Soares et al. (2005) numerically investigated the steady and incompressible flow of power-law fluids across an unconfined, heated circular cylinder to determine the dependence of the individual drag and the heat transfer characteristics, with in the following ranges: Power law indices ($0.5 < n < 1.4$), Reynolds numbers ($5 < Re < 40$), Prandtl numbers ($1 < Pr < 100$) . The momentum and energy equations were solved using a second-order finite difference method to determine the pressure drag and frictional drag as well

as the local and surface-averaged Nusselt numbers and to map the temperature field near the cylinder. The study of flow parameters showed that the frictional drag component increased with the flow-behaviour index n and that the dependence of this component on n increased with Reynolds number.

Bharti et al. (2005) studied forced convection heat transfer in non-Newtonian power law fluids past an unconfined circular cylinder symmetrically placed in between two parallel boundaries in the steady cross flow regime, for following ranges of conditions: Reynolds number up to 40, Power law index (0.8, 1.0, 1.2), Prandtl numbers (1, 10). They also conducted a study of streamlines, isotherms, distribution of vorticity and viscosity on the surface of cylinder. Flow and heat transfer is governed by the continuity, momentum and thermal energy equations. They solved the equations using semi-implicit FVM and QUICK scheme. The vorticity and viscosity show qualitatively similar dependence on the power law index and separation point shows the highest but opposite magnitude of the viscosity for shear thinning and shear thickening fluids.

Bharti et al. (2006) studied forced convection heat transfer in incompressible power law fluids from a heated circular cylinder in the steady cross flow regime numerically by solving momentum and thermal energy equations using a finite volume method and the QUICK scheme on a non-uniform Cartesian grid for following ranges of conditions: Reynolds number ($5<Re<40$), Power law index ($0.6<n<2$), Prandtl number ($1<Pr<1000$). Numerical results were used to develop simple correlations as functions of pertinent dimensionless variables. Effects of Reynolds number, Prandtl number and Power law index on local Nusselt number were also studied to provide further physical insights. Effects of two types of thermal boundary conditions namely constant temperature and uniform heat flux on surface of cylinder were also presented.

Bharti et al. (2006) solved the momentum equations describing the steady cross-flow of power law fluids across an unconfined circular cylinder using a semi implicit finite volume method. The flow characteristics have been presented for the following ranges of conditions: Reynolds number ($5<Re<40$), Power law index ($0.6<n<1.8$). They detailed that for the wake size showed non monotonous variation with power law index but it did not influence the value of drag coefficient. Pressure coefficient, vorticity and viscosity distributions on the surface of the cylinder were also presented to gain further physical insights into the flow kinematics.

Sivakumar et al. (2006) numerically investigated conditions for the formation of a wake and for the onset of wake instability for the power law fluids over an unconfined circular cylinder by solving continuity and momentum equations using FLUENT 6.3. Effect of power law index on the Reynolds number, Strouhal number and drag coefficient has been presented over a wide range of power law index ($0.3>n>1.8$) thereby establishing limits of flow without separation and for the steady symmetric flow regimes respectively. Both shear thinning and thickening seem to lower the values of critical Reynolds number denoting the onset of wake instability as compared to that for the Newtonian fluids. The effect was seen to be more prominent for shear thickening fluids. Corresponding values for critical Strouhal number and drag coefficient have been presented for critical values of Reynolds number.

Bharti et al. (2007) studied forced convection heat transfer from an unconfined circular cylinder in the steady cross-flow regime used finite volume method for following ranges of conditions: Reynolds number ($10<Re<45$), Prandtl number ($0.7<pr<400$). Numerical results were used to develop various correlations for Nusselt number as a function of dimensionless variables. Besides average Nusselt number, effects of Reynolds number, Prandtl number and thermal boundary conditions on temperature field near the cylinder were also presented to provide further insights into the nature of flow. Rate of heat transfer was found to increase

with increase in Reynolds number and Prandtl number. Uniform heat flux condition always showed higher value of heat transfer coefficient than the constant wall temperature at the surface of cylinder for the same Reynolds and Prandtl number.

Bharti et al. (2007) made contribution in the Poiseuille flow of incompressible power-law fluids past a circular cylinder. They placed a circular cylinder midway between two parallel plates and investigated the continuity and momentum equations using FLUENT. Extensive results highlighting the roles of the Reynolds number (Re), the power-law index (n), and the blockage ratio on flow characteristics have been presented over wide ranges of conditions ($1 < Re < 40$, $0.2 < n < 1.9$, and $1.1 < \hat{a} < 4$). For a fixed value of the blockage ratio, the drag coefficient increases as the shear-thickening ($n > 1$) tendency of the fluid increases, whereas shear-thinning ($n < 1$) fluid behaviour shows the opposite dependence. At small Re, this effect is observed to be very strong and it gradually diminishes as Re increases. The effect of Re diminishes for $n > 1$with a decrease in â, whereas the dependence becomes stronger for $n < 1$. In addition, the streamline and pressure profiles have also been presented to provide further insights into the detailed kinematics of the flow. The wake size is also observed to increase as the flow power law index (n) decreases. Because of wall effects, the flow separation seems to be delayed in shear-thickening fluids, whereas the opposite trend was observed in shear-thinning fluids. The pressure profiles are observed to be similar to that for an unconfined flow. The dependence of the pressure coefficient on the flow behaviour index intensifies in shear-thickening fluids with a decrease in the value of blockage ratio.

Dhiman et al. (2007) studied laminar mixed convection flow and heat transfer in case Newtonian and power-law fluids from a heated square cylinder. The momentum and energy equations along with the Boussinesq approximation were used to simulate the buoyancy effects. A semi-explicit finite volume method with non-uniform grid has been used for the following

range of conditions: Reynolds number 1–30, power-law index: 0.8–1.5, Prandtl number 0.7–100, Richardson number 0–0.5. The drag coefficient and the Nusselt number have been reported for a range of values of the Reynolds number, Prandtl number, and Richardson number for Newtonian, shear-thickening $n<1$ and shear thinning $n<1$ fluids. In this study, the effects of Prandtl number and of power law index on the Nusselt number have been found to be more pronounced than that of buoyancy parameter $Ri<0.5$ for a fixed Reynolds number in the steady cross-flow regime $Re<30$. The total drag coefficient and the average Nusselt number show weak dependence on the Richardson number in the steady cross-flow regime.

Soares et al. (2009) studied mixed convection heat transfer characteristics from a circular cylinder immersed in power law fluids. They numerically solved the continuity, momentum, and thermal energy equations using a second-order finite difference method to obtain surface vorticity patterns and determine the local and surface averaged values of the Nusselt number for following ranges of conditions: Power law index (0.6, 0.8, 1, 1.6), Prandtl number (1,100), Reynolds number (1- 30), Richardson number (0, 1, 3). In this work, the drag coefficient was found to be a decreasing function of Reynolds number and power law index for all values of Richardson number. The increasing degree of mixed convection was found to distort streamline patterns anticlockwise, to shift anticlockwise the position of power law viscosity maxima and minima, and change the vorticity profile at the cylinder surface. The effects of mixed convection on heat transfer characteristics were generally more significant at lower values of power law index.

Srinivas et al. (2009) considered the case of an isothermally heated horizontal cylinder immersed in compressible power law fluid through which mixed convective heat transfer occurs. In steady flow, both imposed flow and buoyancy force is in same direction called as aiding buoyancy. The momentum and thermal equations for power law fluid were solved numerically using finite volume based FLUENT 6.3 for the following ranges of conditions: Richardson number $0 < Ri < 2$; Power-law index $0.2 < n < 1.8$;

Reynolds number $1 < Re < 40$; and Prandtl number $1 < Pr < 100$. Under all these condition, they observed that wake size decreases with increasing values of Richardson number and/or Prandtl number and surface pressure coefficient decreases with the increasing Reynolds and Prandtl number whereas local and average Nusselt numbers increases with increasing values of Reynolds, Prandtl, and Richardson numbers.

Singh et al. (2010) simulated the flow across a circular cylinder placed symmetrically in a channel with a second-order accurate, unstructured grid, finite volume collocated Navier–Stokes solver for different values of Reynolds number (45, 100, 150, 200 and 250) with the normalized channel height (H/D) varying from 2.0 to 8.0. Wall proximity was found to have considerable influence on the location of the separation points and length of the recirculating zones. The separation points were found to move rearward resulting in a shorter wake with the decreasing values of channel height. The presence of the sidewalls also delayed the transition from a steady flow with closed attached wake to an unsteady flow. The normalized critical gap is less than 0.5 at Reynolds numbers of 150, 200 and 250. When the channel height was more than the critical value, vortex shedding occurred as in unbounded flow. Due to the interaction between the vortices in the wall boundary-layers and cylinder wake, the vortex street disappeared at a little downstream when the channel height was little more than the critical value. The shed vortices were engulfed by the boundary-layers. This process occurred till the normalized channel height is about 4.0 at Reynolds number of 100 and 150, and is about 3.0 for the higher Reynolds numbers. The length of the distinct vortex street increased with Reynolds number and channel height. The mean drag coefficient and Strouhal number in the unsteady flow regime were found to decrease with increasing channel height. Both the parameters are significantly large when the channel height is small. The Strouhal number was practically independent of Reynolds number at small values of H/D. The wall effect on these global parameters was most pronounced and severe for H /D ratio 4.0 and progressively decreased thereafter.

Patnana et al. (2010) studied numerically two-dimensional (2D), unsteady flow from an unconfined circular cylinder. The governing equations, continuity, momentum and thermal energy have been solved using a finite volume method based solver - FLUENT 6.3 for following ranges of conditions: Power law index(0.4 <n <1.8), Reynolds number (40 <Re <140), Prandtl number (1 <Pr <100). Depending upon the value of the power law index(n), flow transition from being steady to unsteady occurs somewhere in the range 33 < Re < 50, the fully developed periodic behaviour is seen only beyond the critical value of the Reynolds number (Re). Observation is that the average Nusselt number increases with Reynolds and/or Prandtl numbers, irrespective of the value of the flow behaviour index. The effect of power-law index on the heat transfer characteristics is seen to be stronger in shear-thinning fluids than that compared to the shear thickening fluids.

Rao et al. (2011) solved numerically momentum and heat transfer equations for flow across a square cylinder. The main emphasis of the work was to delineate the values of the Reynolds number denoting the onset of flow separation and the limits of the steady flow regime for both shear-thinning and shear-thickening type fluids. The flow characteristics have been presented for the following ranges of conditions: Reynolds number (0.1<Re<40), Power law index (0.2<n<1.4) & Prandtl number (0.7<Pr<100). Effects of Reynolds number, Prandtl number and Power law index on local Nusselt number were also studied to provide further physical insights.

Chandra et al. (2012) investigated mixed convection from a heated semi-circular cylinder to power-law fluids in the steady flow regime. The momentum and thermal energy equations have been solved numerically over the following ranges of conditions: 0.6< Ri <2, 0.2< n <1.8,1< Re <30 and 1< Pr <100. The combined effects of the forced and free convection on the flow and thermal fields are visualized in terms of the streamline and isotherm contours. Further insights are provided in terms of the distribution

of pressure coefficient and local Nusselt number along the cylinder surface. The influence of the power-law index is strongly modulated by the value of the Reynolds number. Between the above mentioned range of conditions it was found that At low Reynolds numbers, such as Re = 1, the local value of the Nusselt number is found to be maximum at corners and for high values of the Reynolds number, it shifts towards the front stagnation point. The average Nusselt number increases with an increase in the value of the Reynolds number, Prandtl number and Richardson number.

Sharma et al. (2012) numerically studied mixed convection flow and heat transfer across a square cylinder under the influence of aiding buoyancy at low Reynolds numbers. (Re = 1-40, Ri = 0-1). The semi-explicit finite volume method was implemented on the collocated grid arrangement is used to solve the governing equations along with the appropriate boundary conditions.. It was found that onset of flow separation occurs between Re = 1–2, between Re = 2–3 and between Re = 3–4 for Ri = 0, 0.5 and 1, respectively. The flow was found to be steady for the range of conditions studied here. The friction, pressure and total drag coefficients were found to increase with Richardson number, i.e., as the influence of aiding buoyancy increases drag coefficients increase at the constant value of the Reynolds number. The temperature field around the obstacle was presented by isotherm contours at the Prandtl number of 0.7 (air). The local and average Nusselt numbers were calculated to give a detailed study of heat transfer over each surface of the square cylinder and an overall heat transfer rate and it was found that heat transfer increases with increase in Reynolds number and/or Richardson number.

2.5 Summary of Literature Review

From the analysis of the literature presented in previous section, it was observed that there have been detailed investigations on the forced convection flow and heat transfer for a circular cylinder submerged in the power-law fluid medium. At high Reynolds numbers, heat transfer occurs mainly by forced convection. As the Reynolds number of the flow is reduced, the natural convection gradually increases. The importance of mixed convection is gauged by the value of the Richardson number ($Ri = Gr/Re^2$). At $Ri \rightarrow 0$, forced heat transfer occurs and at $Ri \rightarrow \infty$, free heat transfer occurs. Mixed convection occurs in between these two limits (Soares et al., 2009). There have been very few studies which deal with the mixed convection (aiding buoyancy) from a circular cylinder in power-law fluids (Bharti el al., 2009, Soares et al., 2009). However, there is clear indication of the gap in the literature in terms of the investigation for other flow configurations for the mixed convection flow. Thus, it constitutes the aim of the present work.

Table 1 Summary of Literature Review

Author	Parameter ranges	Remarks
Soares et al. (2005)	$0.5 < n < 1.4$ $5 < Re < 40$ $1 < Pr < 100$	Flow parameters showed that the frictional drag component increased with the flow-behaviour index n and that the dependence of this component on n increased with Reynolds number.
Bharti et al. (2005)	Re = up to 40, n = 0.8, 1.0, 1.2 Pr = 1, 10	The local and average Nusselt was seen to be higher in shear-thinning fluids than that Newtonian and shear-thickening. Both the local and average Nusselt number increase with a decrease in power-law index and/or an increase in the Prandtl number.

Bharti et al. (2006)	5<Re<40, 0.6<n<2, 1<Pr<1000	The drag coefficient is always seen to decrease with an increase in power law index for n ≥ 1.5.
Bharti et al. (2006)	5<Re<40 0.6<n<2	Shear thinning behaviour of fluids decreases size of recirculation zone and delays the separation and The drag coefficient is always seen to decrease with an increase in power law index for n ≥ 1.5.
Sivakumar et al. (2006)	0.3<n<1.8	Shear thinning and shear thickening seem to lower the values of critical Reynolds number denoting the onset of wake instability as compared to that for the Newtonian fluids.
Bharti et al. (2007a)	10<Re<45 Pr = 0.7<pr<400	Rate of heat transfer was found to increase with increase in Reynolds number and Prandtl number uniform heat flux condition.
Bharti et al. (2007b)	1 < Re < 40, 0.2 < n < 1.9, and 1.1 < ß < 4).	The drag coefficient increases as the shear-thickening (n > 1) tendency of the fluid increases and vice versa for shear thinning fluids(n<1)
Soares et al. (2009)	Re =1-30, n = 0.6, 0.8, 1, 1.6, Pr =1,100 Ri =0, 1, 3	The drag coefficient was found to be a decreasing function of Reynolds number and power law index for all values of Richardson number.

Srinivas et al. (2009)	$0 < Ri < 2$; $0.2 < n < 1.8$; $1 < Re < 40$; $1 < Pr < 100$	Wake size decreases with increasing Richardson number and/or Prandtl number and surface pressure coefficient decreases with the increasing Reynolds and Prandtl numbers whereas local and average Nusselt numbers increase with increasing values of Reynolds, Prandtl, and Richardson numbers.
Patnana et al. (2010)	$40 < Re < 140$ $0.4 < n < 1.8$, $1 < Pr < 100$	The average Nusselt number increases with Reynolds and/or Prandtl numbers, irrespective of the value of the flow behaviour index.
Rao et al. (2011)	$0.1 < Re < 40$ $0.2 < n < 1.4$ $0.7 < Pr < 100$	The Nusselt number shows positive dependence on both the Reynolds and Prandtl numbers. Also, shear - thinning characteristics can augment the rate of heat transfer by up to 100% under appropriate conditions.
Chandra et al. (2012)	$0.6 < Ri < 2$ $0.2 < n < 1.8$ $1 < Re < 30$ $1 < Pr < 100$	Between the mentioned range of conditions it was found that, at low Reynolds numbers, such as Re = 1, the local value of the Nusselt number is found to be maximum at corners and for high values of the Reynolds number, it shifts towards the front stagnation point. The average Nusselt number increases with an increase in the value of the Reynolds number, Prandtl number and Richardson number.

Sharma et al. (2012)	Re = 1-40, Ri = 0-1	The flow was found to be steady for the range of conditions studied here. The friction, pressure and total drag coefficients were found to increase with Richardson number, i.e., as the influence of aiding buoyancy increases drag coefficients increase at the constant value of the Reynolds number.

2.6 Objectives of the Present Work

The following objectives are set up to investigate the influence of fluid behaviour in the mixed convection flow across an isothermally heated circular cylinder:

1) To investigate the effects of temperature and shear-dependent dependent viscosity on the local and global momentum and heat transfer characteristics. This investigation requires the following steps:
    a. Approximation of two-dimensional (2D), steady flow of an incompressible non-Newtonian flow over an infinitely long circular cylinder.
    b. Solve the continuity, momentum, and thermal energy equations for non-Newtonian fluid for the above defined problem and geometric situations using FLUENT.
2) To obtain the influences of the Reynolds number (Re), Prandtl number (Pr), power-law index (n), Richardson number (Ri) and temperature thinning index (b) on the following:
    - Drag coefficient (C_D) & avrage Nusselt number (Nu)
    - Detailed local and global kinematics of momentum and heat transfer

CHAPTER – 3

MATHEMATICAL FORMULATION & GOVERNING EQUATIONS

This chapter discusses the geometrical details of the flow configuration along with the simplifying assumptions, followed by the governing differential equations and the appropriate boundary conditions used.

3.1 Problem Statement

In this study, the 2-D unconfined flow of an incompressible power law fluid across a circular cylinder is investigated as shown in Fig. 3. This obstacle of circular cross-section is exposed to uniform flow (having a velocity U_∞ and temperature T_∞) at the inlet. The cylinder is placed at an upstream distance L_u from the inlet and a downstream distance of L_d from the outlet. The total length of the computational domain is L in the axial direction and a height H in the lateral direction. The surface of the cylinder is taken to be at a constant wall temperature (T_w). The thermo-physical properties (except viscosity) of the streaming fluid are assumed to be independent of temperature.

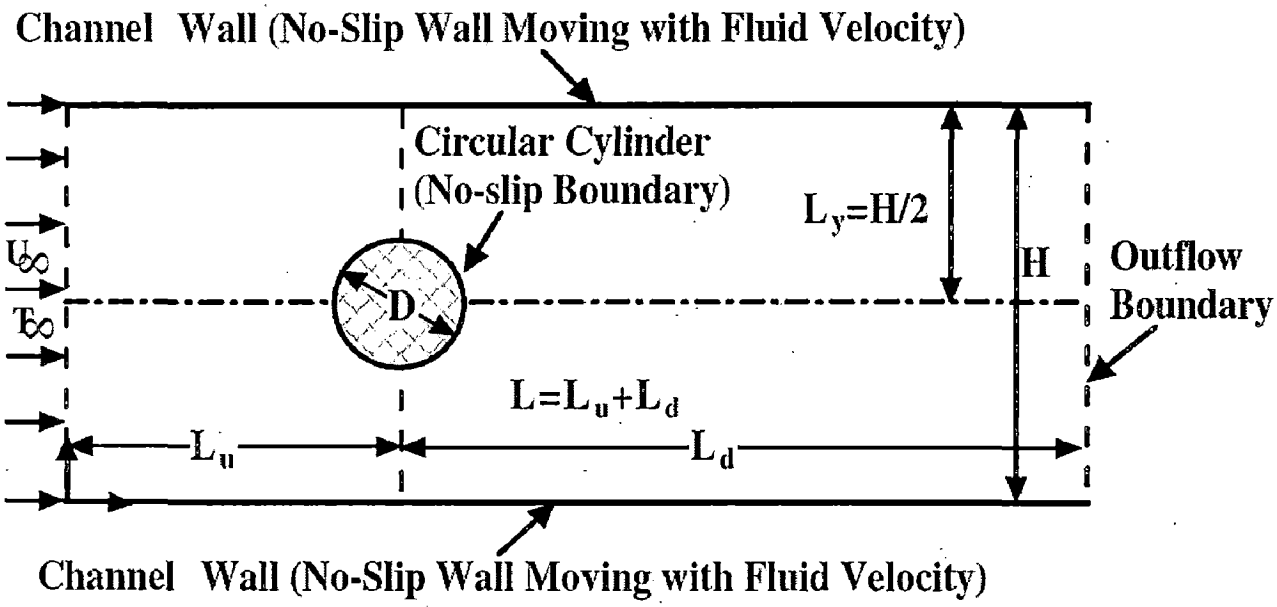

Figure 3 Schematics of the flow around an unconfined circular cylinder

3.2 Mathematical Formulation

The flow and heat transfer problems are governed by the continuity, momentum and thermal energy equations.

The continuity, momentum, and thermal energy equations (Srinivas et al., 2009) are as follows:

Continuity equation

$$\frac{\partial U_x}{\partial x}+\frac{\partial U_y}{\partial y}=0 \tag{1}$$

X-component of momentum equation:

$$\rho\left(U_x\frac{\partial U_x}{\partial x}+U_y\frac{\partial U_x}{\partial y}\right)=-\frac{\partial p}{\partial x}+\left(\frac{\partial \tau_{xx}}{\partial x}+\frac{\partial \tau_{yx}}{\partial y}\right) \tag{2}$$

Y-component of momentum equation:

$$\rho\left(U_x\frac{\partial U_y}{\partial x}+U_y\frac{\partial U_y}{\partial y}\right)=-\frac{\partial p}{\partial y}+\left(\frac{\partial \tau_{xy}}{\partial x}+\frac{\partial \tau_{yy}}{\partial y}\right)+\rho g_y \tag{3}$$

Thermal energy equation:

$$\rho c_p\left(U_x\frac{\partial T}{\partial x}+U_y\frac{\partial T}{\partial y}\right)=k\left(\frac{\partial^2 T}{\partial x^2}+\frac{\partial^2 T}{\partial y^2}\right) \tag{4}$$

Where

U_x: Velocity in x direction (m/s)

U_y: Velocity in y direction (m/s)

ρ: Density of fluid (kg/m^3)

T: Temperature (K)

p: Pressure (Pa)

C_p: Heat Capacity (J/kg K)

k: Thermal Conductivity (W/m^2 K)

τ: Shear Stress (Pa)

Relation between the components of extra stress tensor and rate of deformation tensor

$$\tau_{ij} = 2\mu\varepsilon_{ij} \text{ Where } (i, j) = (x, y) \tag{5}$$

- Rate of deformation tensor is given as

$$\varepsilon_{ij} = \frac{1}{2}\left(\frac{\partial U_i}{\partial j} + \frac{\partial U_j}{\partial i}\right) \tag{6}$$

- Power law fluid:

$$\mu = m(I_2/2)^{(n-1)/2} \tag{7}$$

$$I_2 = 2(\varepsilon_{xx}{}^2 + \varepsilon_{xy}{}^2 + \varepsilon_{yx}{}^2 + \varepsilon_{yy}{}^2) \tag{8}$$

Where,

m = power law consistency index

n = power law index of the fluid

I_2 = second invariant of the rate of strain tensor

Since, Boundary conditions for the circular cylinder are written as follows:

- Inlet boundary condition: $U_x = U_\infty$, $U_y = 0$, $T = T_\infty$
- On Surface of the cylinder : Standard no-slip condition and constant temperature

Dirichlet boundary conditions

$U_x = 0$, $U_y = 0$, $T = T_w$

Exit boundary condition:

Neumann boundary condition

$$\frac{\partial U_x}{\partial y} = 0 \ , \ \frac{\partial U_y}{\partial y} = 0 \quad \frac{\partial T}{\partial y} = 0 \tag{9}$$

- At plane of symmetry (x=0): The symmetric flow condition is imposed.

$$\frac{\partial U_x}{\partial y} = 0 \quad U_y = 0 \quad \frac{\partial T}{\partial x} = 0 \tag{10}$$

The effect of temperature dependence on viscosity (Soares et al., 2010) are assumed to be in the form

$$\mu = Ae^{\frac{E}{R\theta}} \tag{11}$$

where θ(K) is the temperature, R the molar gas constant, and activation energy E needs to be independent of viscosity. In practice, most fluids do obey this form of temperature dependence, albeit over varying ranges of temperature intervals.

The following approximation is used for the dimensionless viscosity η:

$$\eta = \frac{\mu}{\mu_\infty} = \frac{e^{\frac{E}{R\theta}}}{e^{\frac{E}{RT_\infty}}} \approx e^{-bT} \tag{12}$$

The temperature thinning index (b) is given by

$$b = \frac{E}{R\,T_0}\frac{T_w - T_\infty}{T_\infty} = \ln\frac{\mu_\infty}{\mu_s} \tag{13}$$

Where

T_w Temperature of cylinder (K)

T_∞ Temperature of fluid at inlet (K)

R Universal gas constant

E Activation Energy (J)

The above mentioned governing equations are being solved using commercial fluid dynamics software (FLUENT) on a proper grid

arrangement. The solution of these equations yields the velocity, pressure and temperature fields. These fields are transformed into the useful fluid dynamics variables such as streamlines, drag coefficients and Nusselt number, etc.

3.3 Numerical Solution Methodology

The governing equations for unconfined flow configuration presented have been solved in FLUENT on a non-uniform grid structure using the QUICK (Quadratic Upwind Interpolation for Convective Kinematics) scheme. The non-uniform grid was generated in the commercial grid generator GAMBIT 2.4.6.

The ensuing section discusses in detail the steps involved in grid generation and the solution procedure used.

3.4 Mesh Generation

The unstructured "quadrilateral" cells of non-uniform grid spacing were generated using the commercial grid tool GAMBIT 2.3.16. The region near the cylinder is given fine meshing to observe the effects around cylinder more vividly and the regions away the cylinder are meshed in somewhat coarser (as compared with cylinder proximity) to save the computational time as in fig.3.

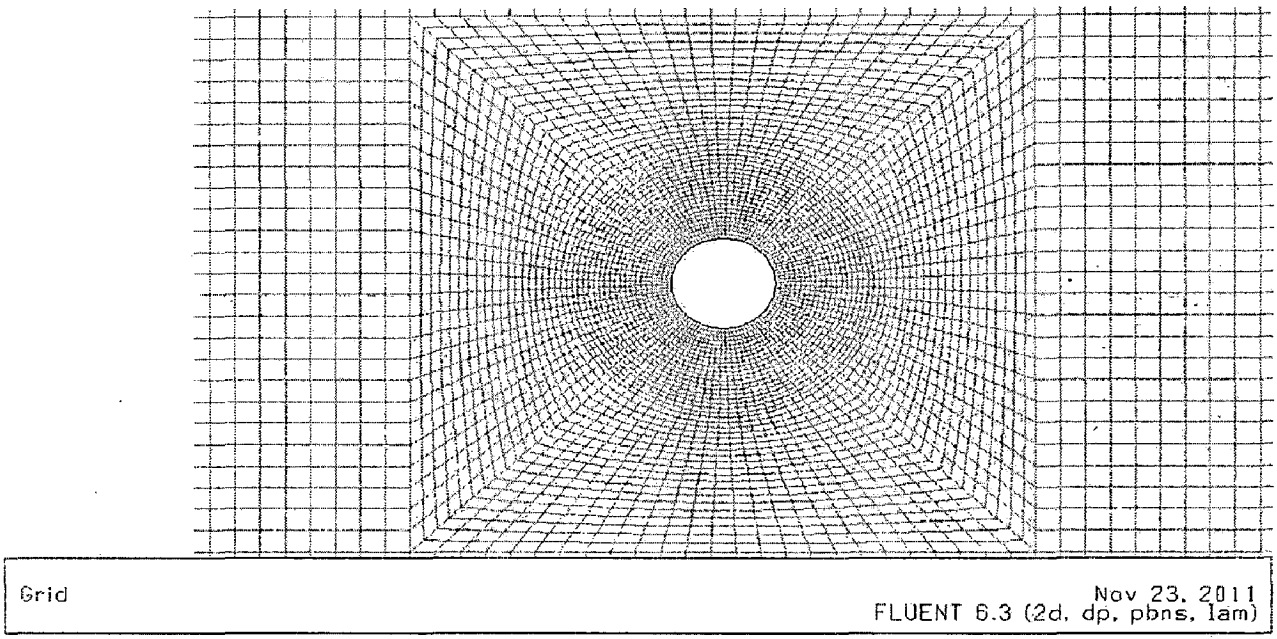

Figure 4 Mesh of the given Problem Statement generated in Gambit 2.3.16

The following boundary types have been specified:

WALL - Upper wall, Lower wall, Cylinder.

VELOCITY_INLET – Inlet.

OUTFLOW – Outlet

The generated mesh is exported to the commercial solver FLUENT

The commercial CFD package FLUENT 6.3 has been used to solve the governing equations. A third order accurate QUICK (Quadratic Upwind Interpolation for Convective Kinematics) scheme has been used to discretize the convective terms in the momentum and thermal energy equations.

CHAPTER – 4

RESULTS AND DISCUSSIONS

In this study, flow and heat transfer across a circular cylinder is studied for the following range of conditions: Re = 1-40, Pr = 1-100, n = 0.2-1.8, Ri = 0-3, b = 0-1. Commercial CFD packages FLUENT was used in this study to carry out the calculations. Having fixed the numerical parameters, the accuracy of the solution procedure has been demonstrated further by producing some of the literature values for the unconfined flow and mixed convection heat transfer in power law fluids across a circular cylinder thereby inspiring confidence in the reliability of the solution procedures and the accuracy of results (Soares et al., 2009).

4.1 Domain Independence Study

Domain and grid sizes play a major role on the accuracy of the numerical solution procedure. Hence, it is necessary to investigate the sizes of domain and grids which yield the results free from end effects (domain sizes) and/or numerical instability (appears due to unbalanced grid structures). In this work, first, the domain independence study has been carried out to find the lengths (upstream, downstream and height) which are optimized in such a manner that the computational time and accuracy of results being balanced to each other. The results of domain independence studies are shown in the preceding sections.

The influence of height on the drag coefficients and average Nusselt number is shown in Table 2. In this part of study, a downstream length (L_d) of 80 & upstream length (L_d) of 20 has been fixed while the height varies as 50, 100 and 150 for two values of the Reynolds number (Re = 1, and 40), for three values of the power-law index (n= 0.2, 1 and 1.8) and for two values of the Richardson number (Ri = 0, 3).

Table 2 Influence of Height (H) on Drag coefficient (C_d) and average Nusselt number (Nu) with Re and power law index at Ld = 80 & Lu = 20

		Ri = 0		*Ri = 3*	
Height	*Re (n)*	C_D	*Nu*	C_D	*Nu*
50	1 (1.8)	6.602	3.180	7.2466	3.294
100		6.262	3.151	6.9735	3.276
150		6.245	3.150	6.9557	3.2748
50	1 (1.0)	11.612	3.478	12.0912	3.5342
100		11.048	3.425	11.7128	3.5032
150		11.003	3.421	11.6785	3.5003
50	1 (0.2)	26.184	5.584	26.8823	5.9262
100		25.621	5.421	26.9591	5.9598
150		25.592	5.408	26.9011	5.9383
50	40 (1.8)	1.7376	17.534	1.8224	16.6147
100		1.7032	17.466	1.8142	16.5847
150		1.7017	17.464	1.8098	16.5805
50	40 (1.0)	1.5435	19.807	1.6244	19.9113
100		1.525	19.737	1.6189	19.8991
150		1.524	19.734	1.6191	19.8996
50	40 (0.2)	1.321	29.523	1.1991	24.9888
100		1.306	29.421	1.198	24.994
150		1.298	29.411	1.1974	24.9847

From table 2 it is clear that the influence of the increase in the height on total drag coefficient and Nusselt number is significant for H=50 to H =100, so a height of 100 units is selected.

The influence of downstream length on the drag coefficients is shown in Table 3. In this part of study, an upstream length (L_u) of 20 & Height of 50 has been fixed while the downstream lengths are varies as 80, 120 and 160 for two values of the Reynolds number (Re = 1, and 40), for three values of the power-law index (n= 0.2, 1 and 1.8) and for two values of the Richardson number (Ri = 0, 3).

Table 3 Influence of downstream length on Drag coefficient (C_d) and average Nusselt number (Nu) with Re and power law index (n) at Lu = 20 & H = 50

		***Ri* = 0**		***Ri* = 3**	
L_D	*Re (n)*	C_D	*Nu*	C_D	*Nu*
80	1 (1.8)	6.6002	3.180	7.2466	3.294
120		6.5990	3.179	7.2476	3.2941
160		6.5984	3.179	7.2476	3.2941
80	1 (1.0)	11.612	3.478	12.0912	3.5342
120		11.612	3.478	12.0913	3.5342
160		11.614	3.478	12.0913	3.5342
80	1 (0.2)	26.184	5.584	26.8823	5.9262
120		26.624	5.742	26.9063	5.845
160		26.741	5.936	26.9602	5.9604
80	40 (1.8)	1.7376	17.534	1.8224	16.6147
120		1.7352	17.534	1.8151	16.5836
160		1.7341	17.534	1.8031	16.6242
80	40 (1.0)	1.5435	19.807	1.6244	19.9113
120		1.5435	19.807	1.6245	19.9113
160		1.5435	19.807	1.6244	19.9113
80	40 (0.2)	1.3212	29.523	1.1991	24.9888
120		1.327	29.639	1.1972	24.9829
160		1.330	29.676	1.1966	24.9934

An analysis of Table 3 shows that the increase of downstream length (L_d) from 80 to 120 yields a significant variation as compared to an increment from 120 to 160 in the values of total drag coefficients over the ranges of parameters considered in this work. Therefore, downstream length (L_d) of 120 is sufficient enough to produce the results are free from the end effects. The influence of upstream length on the drag coefficients is shown in Table 4. In this part of study, a downstream length (L_d) of 80 & Height of 50 has been fixed while the upstream lengths are varies as 20, 30 and 40 for two values of the Reynolds number (Re = 1, and 40), for three values of the

power-law index (n= 0.2, 1 and 1.8) and for two values of the Richardson number (Ri = 0, 3).

Table 4 Influence of downstream length on Drag coefficient (C_d) and average Nusselt number (Nu) with Re and power law index at Ld = 80 & H = 50 at Ri =0

		***Ri* = 0**		***Ri* = 3**	
L_u	*Re (n)*	C_D	*Nu*	C_D	*Nu*
20	1 (1.8)	6.602	3.18	7.2466	3.294
30		6.457	3.168	7.0548	3.2791
40		6.425	3.166	7.0335	3.2765
20	1 (1.0)	11.612	3.478	12.0912	3.5342
30		11.464	3.464	11.9518	3.5204
40		11.449	3.463	11.9393	3.5181
20	1 (0.2)	26.184	5.584	26.8823	5.9262
30		27.144	6.025	26.9586	5.9597
40		26.984	5.569	26.9083	5.9427
20	40 (1.8)	1.7376	17.534	1.8224	16.6147
30		1.7204	17.498	1.8122	16.5673
40		1.716	17.489	1.8027	16.5523
20	40 (1.0)	1.5435	19.807	1.6244	19.9113
30		1.5341	19.769	1.6101	19.8769
40		1.5317	19.759	1.6067	19.8684
20	40 (0.2)	1.3212	29.523	1.1991	24.9888
30		1.3201	29.519	1.1196	24.9909
40		1.3122	29.510	1.1999	24.9918

An analysis of Table 4 shows that the increase of upstream length (L_u) from 20 to 30 results in significant variation as compared to an increment from 30 to 40 in the values of total drag coefficients over the ranges of parameters considered in this work. Therefore, upstream length (L_u) of 30 is sufficient enough to produce the results are free from the end effects.

Based on the influence of the domain sizes on the drag coefficients and Nusselt number shown above, the domain size of L_d = 120D, L_u = 30D & H =

100D is resulted in domain free results and therefore has been used in this study to obtain the final results.

4.2 Grid Independence Study

For this study three meshes having different grid sizes were chosen. The number of points on the cylinder were chosen to be 100.

As can be seen from the table 5 there is very little variation in the values of drag coefficient and average Nusselt number on changing the cell size so the mess having coarser spacing and comparable computational time (G2) is chosen.

Table 5 Influence on drag coefficient (C_d) and average Nusselt number (Nu) with Re and power law index for three different grids having dimensions (Ld = 120, Lu = 30 & H = 100)

		***Ri* = 0**		***Ri* = 3**	
	Re (n)	C_D	*Nu*	C_D	*Nu*
G1	1 (1.8)	6.266	3.1518	6.3511	3.232
G2		6.2662	3.1511	6.3579	3.2268
G3		6.2671	3.1433	6.3601	3.2201
G1	1 (1.0)	11.0519	3.426	11.2441	11.0519
G2		11.0578	3.4215	11.2575	11.1027
G3		11.1027	3.421	11.2611	11.1096
G1	1 (0.2)	26.8575	5.9105	26.7967	5.9122
G2		26.0148	5.3323	26.6744	5.8234
G3		26.0109	5.3175	26.6344	5.8097
G1	40 (1.8)	1.7031	17.4667	1.7759	16.5233
G2		1.7038	17.4967	1.7797	15.5674
G3		1.7041	17.5189	1.7801	15.4357
G1	40 (1.0)	1.525	19.7375	1.594	19.8388
G2		1.5239	18.6745	1.5874	18.772
G3		1.5213	18.3359	1.5842	18.709
G1	40 (0.2)	1.2032	23.0817	1.1978	24.9939
G2		1.2	22.7661	1.0703	24.5887
G3		1.1953	21.877	1.0345	22.4322

G1 – Grid 1, G2 – Grid 2 G3 – Grid 3

G1 – 192678 quadrilateral cells
100 points on cylinder with .1D spacing near the cylinder and .24D away from the cylinder

G2 – 198178 quadrilateral cells
100 points on cylinder with .05D spacing near the cylinder and .24D away from the cylinder

G3 – 208378 quadrilateral cells
100 points on cylinder with .02D spacing near the cylinder and .24D away from the cylinder

4.3 FLUENT Methodology

The commercial CFD package FLUENT was used to compute the unconfined flow cases studied in this thesis. FLUENT uses the FVM technique to discretize the governing equations. The FVM discretization process used in FLUENT consist of the

- Subdivision of the flow domain into a set of non-overlapping control volumes (CVs) or cells
- Integration of the conservation equations over cell assuming uniform values of the variables over the entire cell.

FLUENT offers different discretization schemes, namely, first order upwind, second order upwind, power law and QUICK scheme. The QUICK scheme has been used here to discretize the convective term in the momentum equations. The semi implicit method for pressure linked equations (SIMPLE) scheme was used for solving the pressure-velocity coupling.

FLUENT provides the density as constant, ideal-gas, incompressible ideal gas, Boussinesq, piecewise linear, piecewise polynomial, polynomial and any other UDFs. The viscosity model available in FLUENT are constant (Newtonian), piecewise linear, piecewise polynomial, power-law, Sutherland,

kinetic theory, cross, Herschel-Bulkley, Carreau, non-Newtonian power-law and UDFs.

In this work, boussinesq approximation for density and 'non-Newtonian power-law viscosity model (shear rate and temperature dependent) is used. FLUENT solves the system of algebraic equations using the GS point-by-point iterative method in conjunction with the algebraic multi-grid method (AMG) solver. The use of the multi-grid scheme can greatly reduce the number of iterations and CPU time required to obtain a converged solution. A relative convergence criteria of 10^{-9} for the continuity, x- and y-components of velocity and energy were prescribed. In addition, the values of the drag coefficients have also been monitored and when there is no further significant change (less than 10^{-4}) was observed for large number of iterations (>1000), the solution is assumed to be converged.

4.4 Validation of Results

The present numerical solution procedure has been validated by comparing the results obtained in this work with the available literature results. The results obtained for different values of Re and Power law coefficient for different values of Richardson Number were found to be in excellent agreement with the literature values. (Srinivas et al., 2009 & Soares et al., 2009)

Table 6 Comparison of present results with available results from the literature for Ri = 0

Re (n)	C_D (Present Work)	C_D (Srinivas et al., 2009)	*Nu* (Present Work)	*Nu* (Srinivas et al., 2009)
1 (1.8)	6.262	5.838	3.1515	3.1103
1 (1.0)	11.048	10.327	3.425	3.345
1(0.2)	25.621	26.94	5.421	5.49
40 (1.8)	1.7032	1.6609	17.4667	15.66
40 (1.0)	1.525	1.4987	19.7376	17.9168
40 (0.2)	1.306	1.1387	29.421	29.77

Table 7 Comparison of present results with available results from the literature for Ri = 1

Re (n)	C_D (Present Work)	C_D (Soares et al., 2009)	*Nu* (Present Work)	*Nu* (Soares et al., 2009)
1 (1.6)	7.0538	7.44	3.203	3.07
1 (1.0)	11.089	10.42	3.431	3.21
1(0.8)	13.799	12.86	3.642	3.37
30 (1.6)	1.8644	1.89	14.301	13.09
30 (1.0)	1.681	1.69	15.97	15.11
30 (0.8)	1.671	1.68	17.639	16.27

4.5 Drag Coefficients

The hydrodynamic drag force component along the x direction can be expressed in terms of the corresponding drag coefficient C_d, and the present study (Figure 5, 6, 7) shows that an increase in Richardson number from Ri = 0 to 3 resulted in increase in values of C_d with Prandtl number 1-100, Reynolds number 1-40 & b = 0-1 irrespective of the fluid behavior index (n). This trend can safely be ascribed to the increasing distortion of streamlines (thereby sharpening of velocity gradients) near the surface of the cylinder with the increasing value of the Richardson number. For all the aforementioned values of Ri and Pr, the drag coefficient was a decreasing function of Reynolds number (Re) whereas an increasing function of power law index (n). Also on increasing the temperature thinning index from 0 to 1, there was a decrease in the values of drag coefficient. Such effects can be attributed to a reduction in frictional drag component due to the overall decrease in the effective viscosity which resulted from larger temperature thinning index. Furthermore, such dependence of drag coefficient on temperature thinning index became more pronounced as the Prandtl number decreased from Pr = 100 to Pr = 1. Also, the increase in Cd with mixed convection parameter *Ri* became more pronounced with at lower Prandtl number (Pr = 1). For instance, at Pr = 1, Re = 1, n = 1 & b = 1 an increase in Ri from 0 to 3 resulted in an increase in C_d from 8.09 to 11.52 whereas at Pr = 100, Re =1, n =1 & b = 1, the increment was from 9.95 to 10.79.

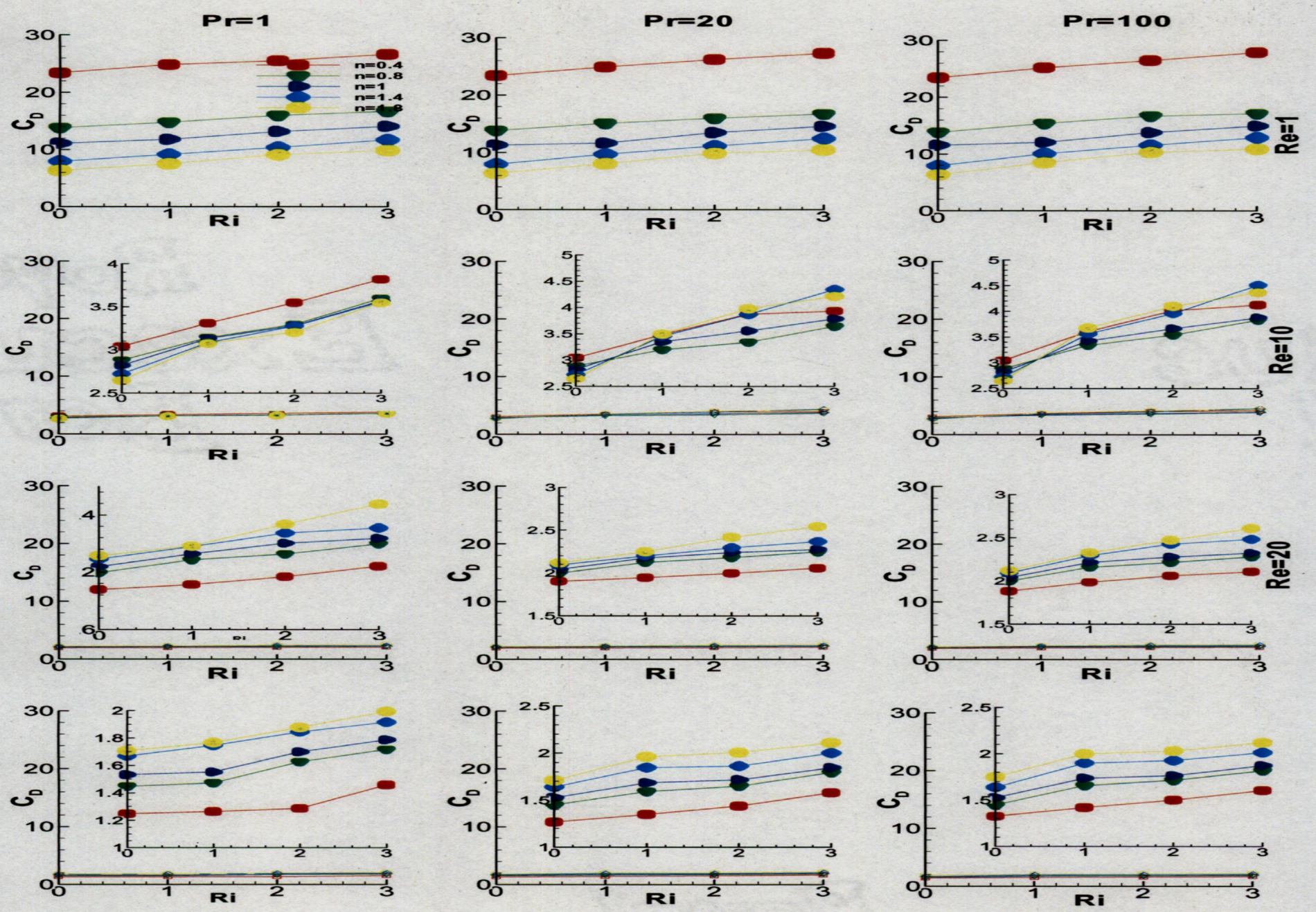

Figure 5 Effect of Richardson number Ri on the total drag coefficient for Re = 1,10,20 and 40, Pr = 1, 20 and 100 and b = 0 for different values of n

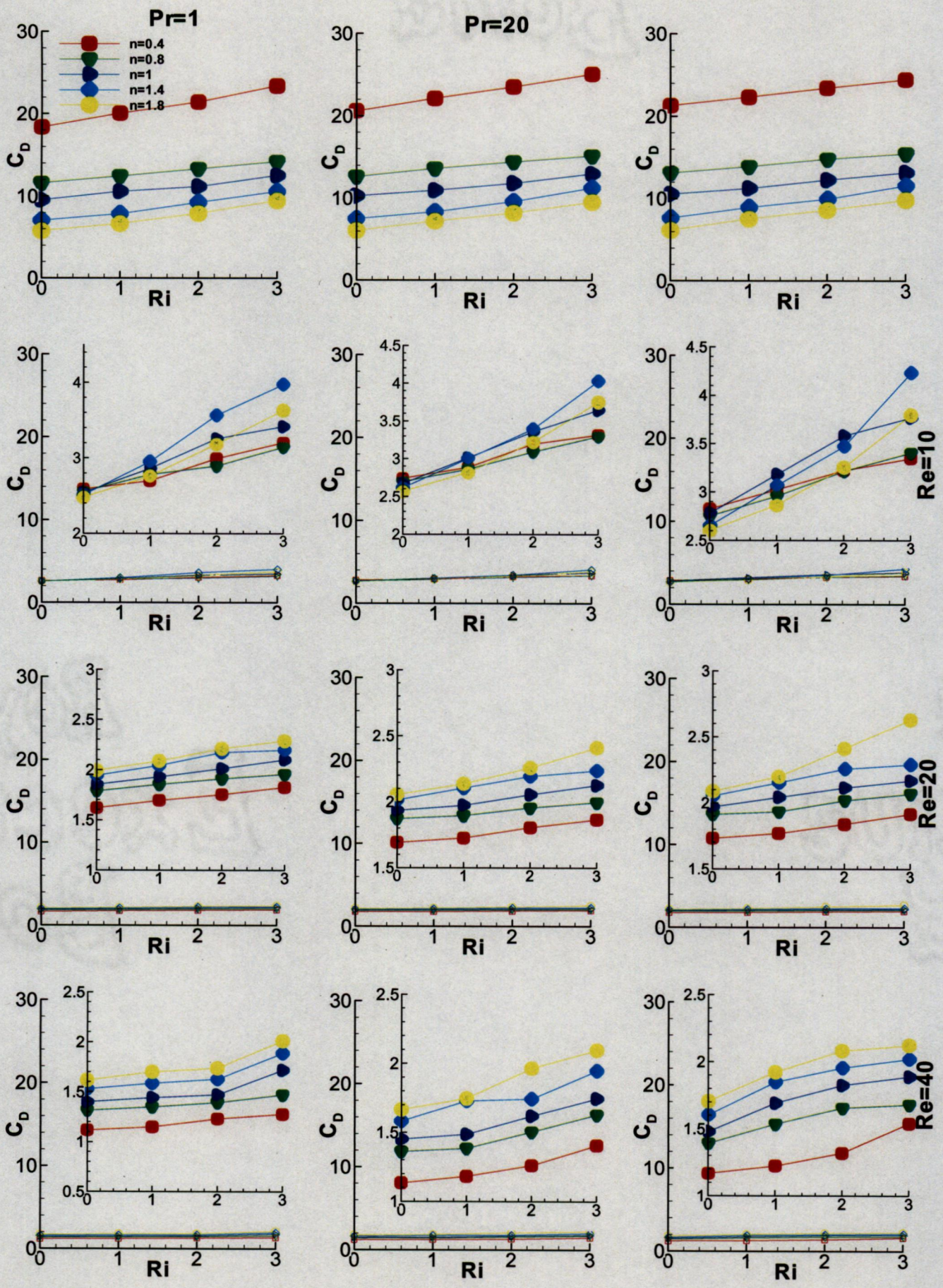

Figure 6 Effect of Richardson number Ri on the total drag coefficient for Re = 1,10,20 and 40,Pr = 1, 20 and 100 and b = 0.5 for different values of n

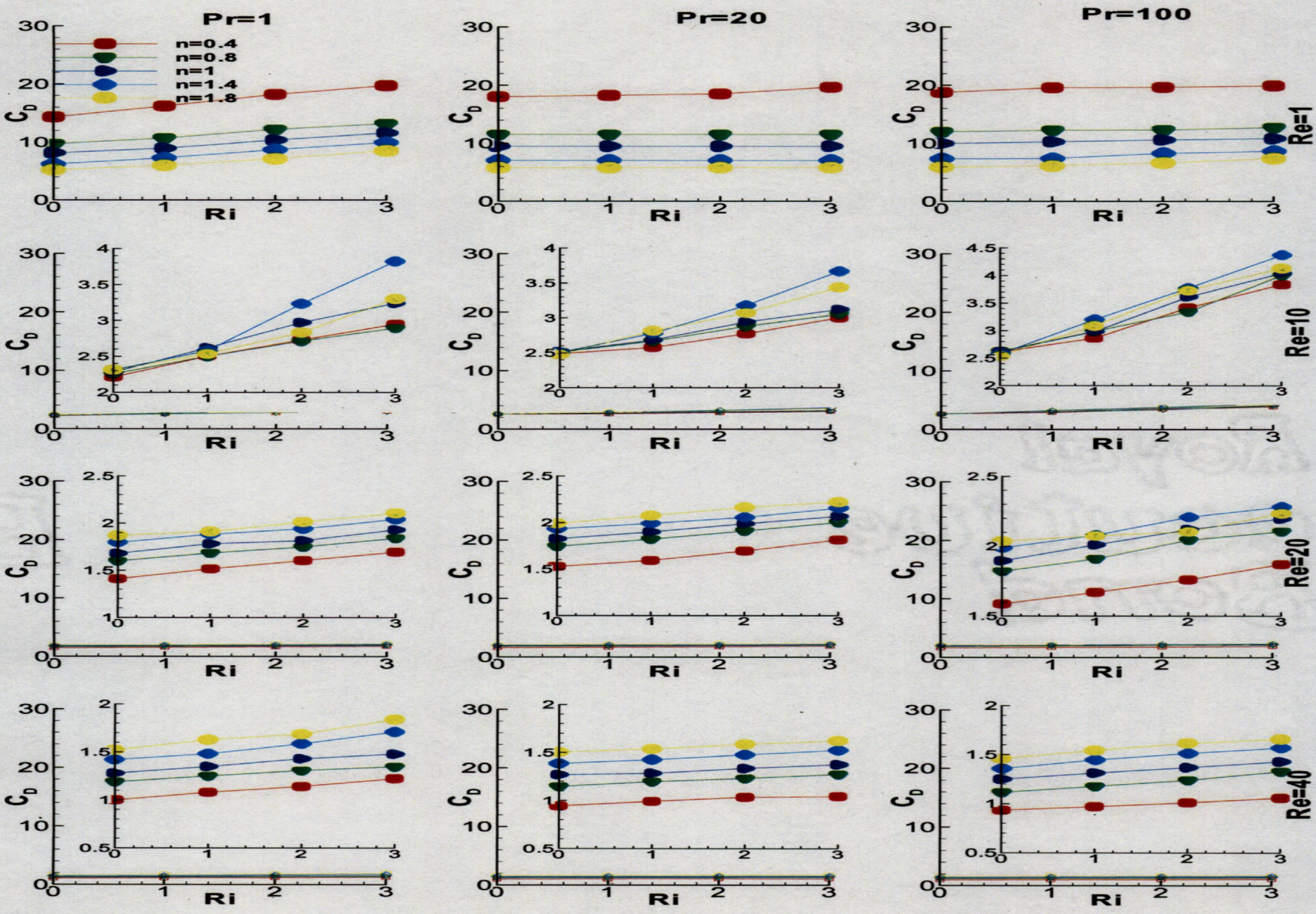

Figure 7 Effect of Richardson number Ri on the total drag coefficient for Re = 1,10,20 and 40, Pr = 1, 20 and 100 and b = 1 for different values of n

4.6Average Nusselt Number

Figure 8, 9, 10 show the functional dependence of the average Nusselt number (*Nu*) on the Reynolds number (*Re*), power-law index (*n*), Richardson number (*Ri*), and Prandtl number (*Pr*)& temperature thinning index (b). The average Nusselt number (*Nu*) shows an increase with Reynolds number (*Re*) and/or Prandtl number (*Pr*) and/or both. For fixed values of the parameters (*Ri, Re, Pr*), the average Nusselt number increases as the fluid behavior changes from Newtonian ($n = 1$) to shear-thinning ($n < 1$); however, the opposite effect is seen in shear-thickening ($n > 1$) fluids. In other words, all else being equal, shear thinning fluid behavior facilitates heat transfer while the shear thickening behavior has deleterious effect on heat transfer. For fixed values of Reynolds number (*Re*), flow behavior index (*n*), and Richardson number (*Ri*), an increasing value of the Prandtl number (*Pr*) also enhances the rate of heat transfer, irrespective of the type of the fluid behavior. The average Nusselt number (*Nu*) values in the mixed convection are always higher than those in the forced convection. For a fixed Reynolds number (*Re*), the average Nusselt number (*Nu*) is seen to increase with increasing Richardson number (*Ri*). It is also seen that the influence of Richardson number (*Ri*) on the average Nusselt number (*Nu*) is more prominent at low Reynolds number than that for high Reynolds numbers. Also increasing the values of temperature thinning index shows an increase in the values of surface averaged Nusselt number. The increase was pronounced for shear thinning fluids as compared to shear thickening fluids. This was mainly due to the lowering of the effective viscosity in shear thinning fluids near the cylinder due to its high temperature.

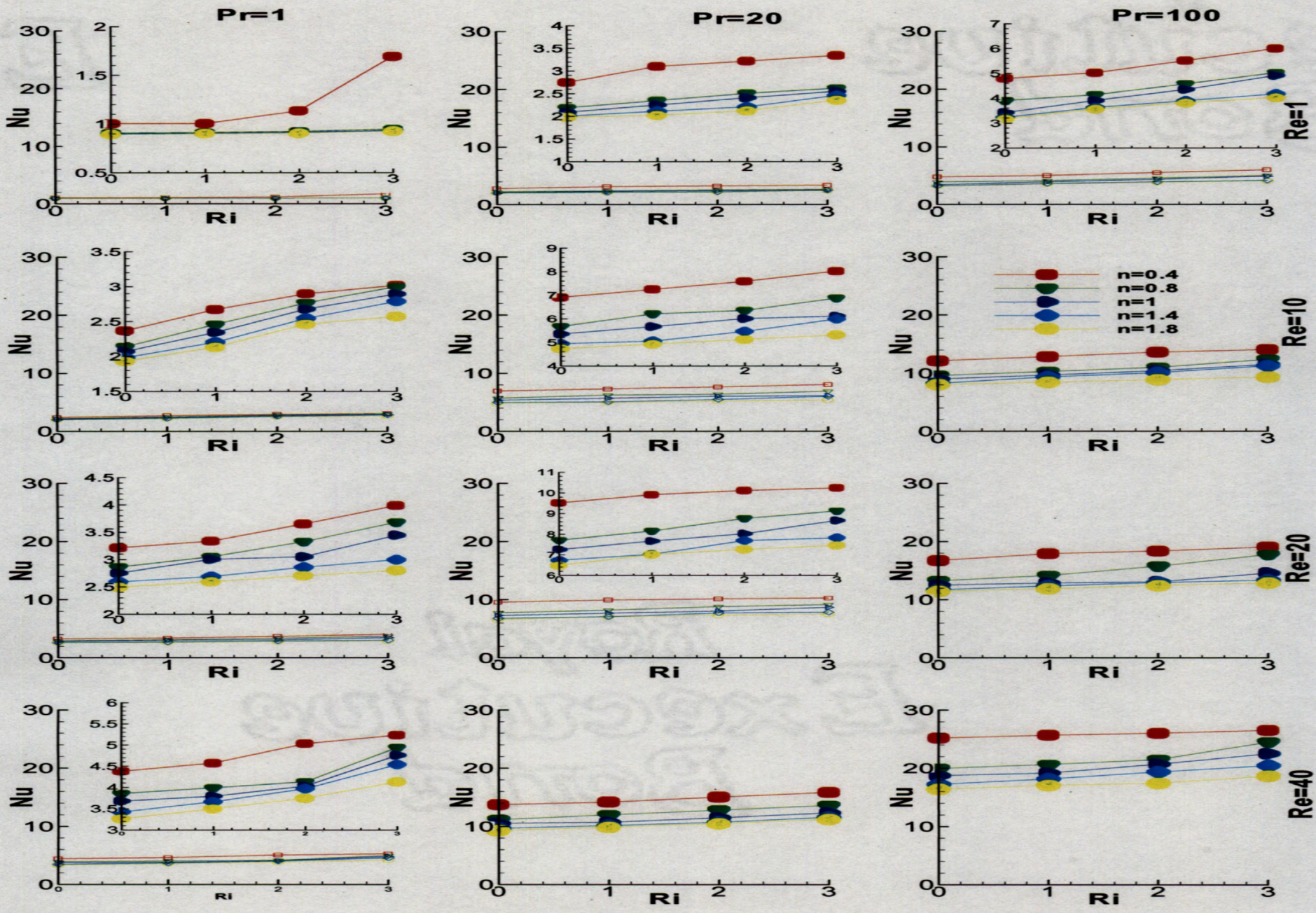

Figure 8 Effect of Richardson number Ri on the surface averaged Nusselt number for Re = 1,10,20 and 40, Pr = 1, 20 and 100 and b = 0 for different values of n

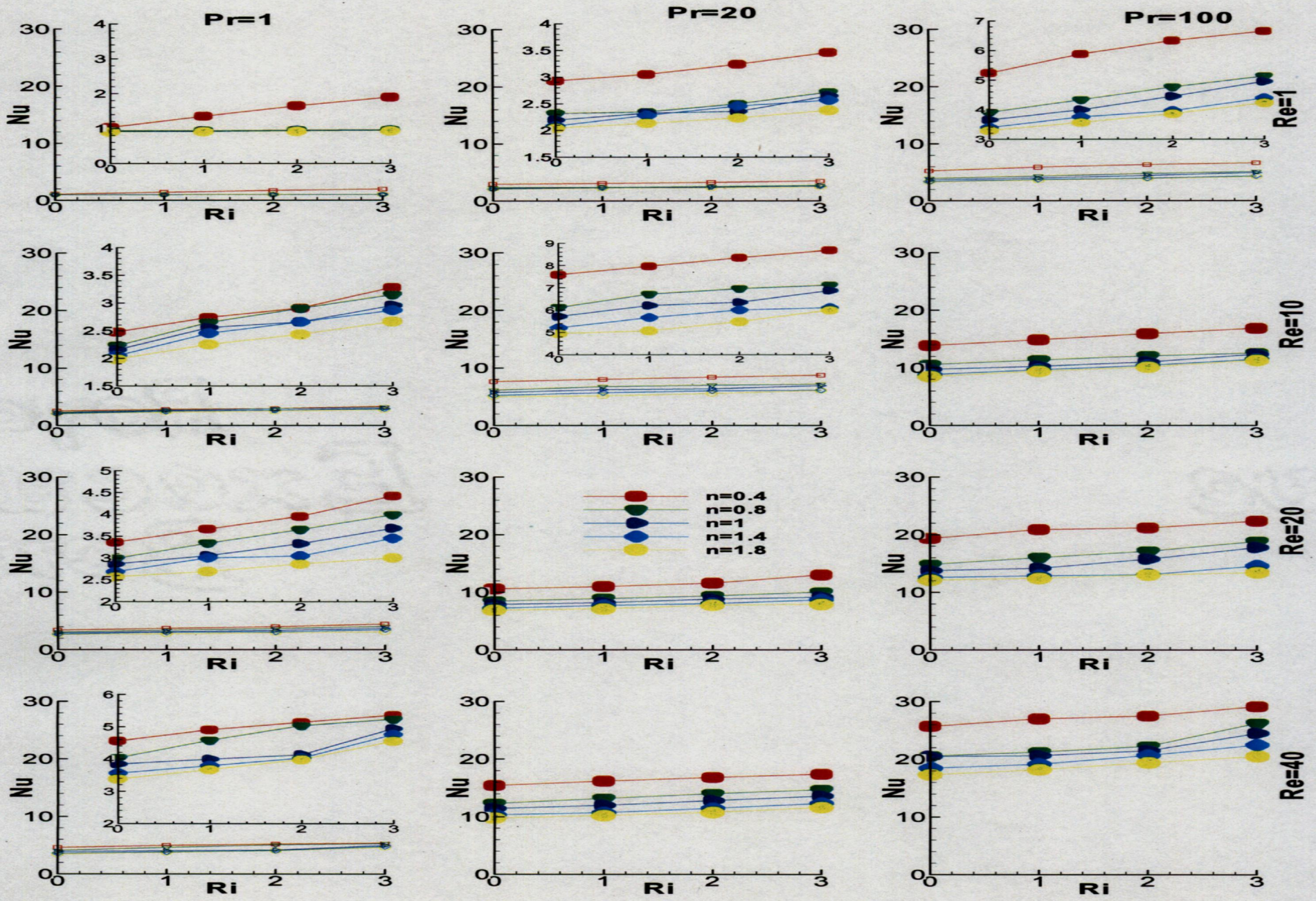

Figure 9 Effect of Richardson number Ri on the surface averaged Nusselt number for Re = 1,10,20 and 40, Pr = 1, 20 and 100 and b = 0.5 for different values of n

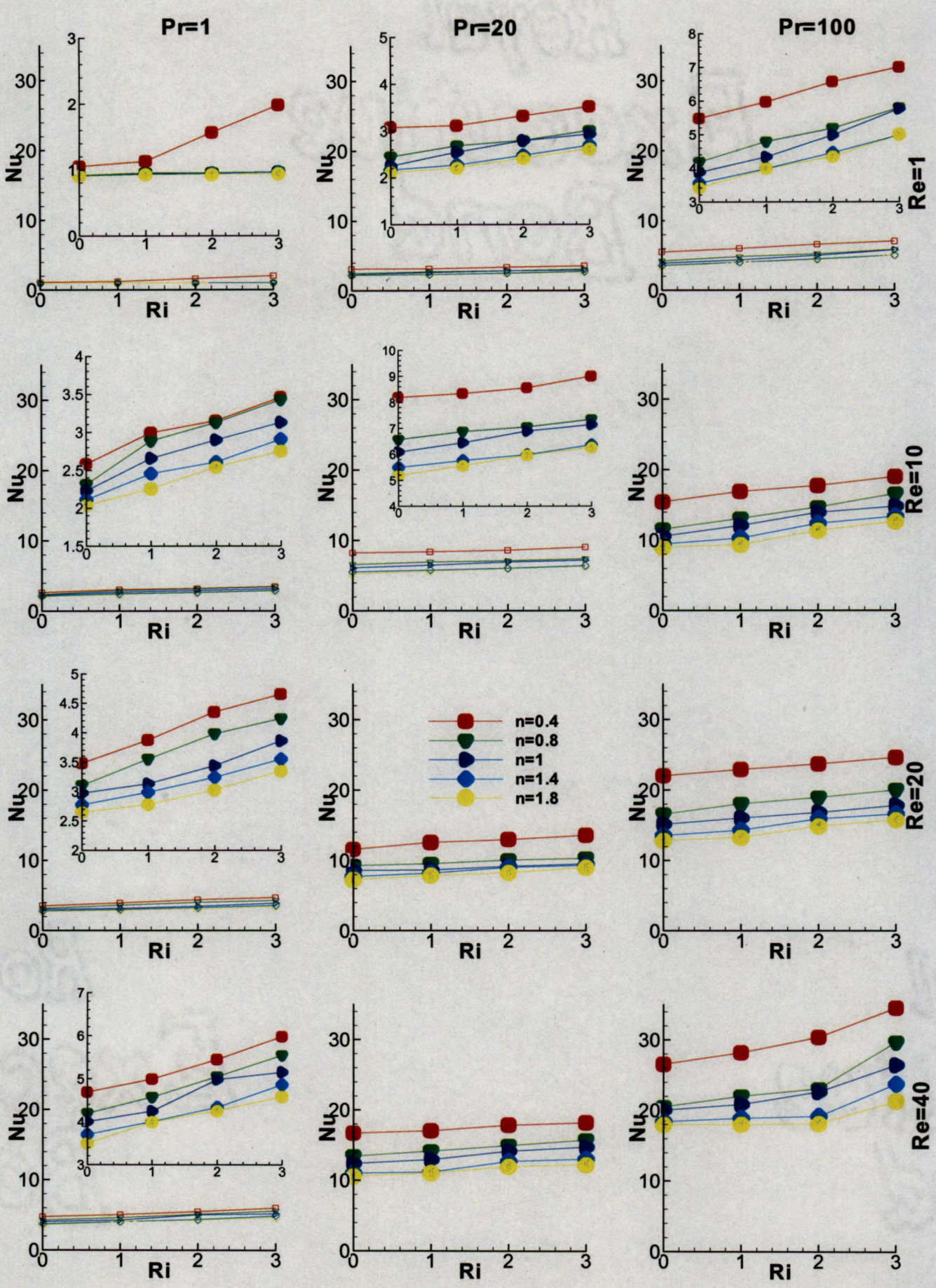

Figure 10Effect of Richardson number Ri on the surface averaged Nusselt number for Re = 1,10,20 and 40, Pr = 1, 20 and 100 and b = 1 for different values of n

4.7 Streamline Patterns

Representative streamline patterns close to the cylinder for Reynolds numbers Re = 1 and 40, Richardson numbers Ri = 0, 1, and 3, Prandtl number Pr = 1and 100, and power law index (n) = .4 , 1 and 1.8 are shown in figures 11 and 12. The main effect of mixed convection term was a loss of symmetry of the streamline patterns, which are known to be symmetrical in the absence of mixed convection, as shown in figures 12 and 13. Such symmetry-breaking was in part characterized by the presence, in the streamline patterns, of a positive slope which increased with the increasing values of the Richardson number Ri. While such upward slope is not seen in pure forced convection, i.e. at Ri = 0, once the mixed convection term was introduced, the positive slope was found to increase with the value of the power law index. The present study also showed that such positive slope became less pronounced at higher values of Re and Pr, so that at Re = 40 and Pr = 100, it was no longer observed. It is so in part due to the thinning of the thermal boundary layer at high Prandtl number and due to the increasing contribution of convection with Reynolds number. For Re = 40, in the absence of buoyancy effects (Ri = 0), the flow separates from the trailing edge of the cylinder to form two symmetrical vortices behind it. Also, it is clear from these figures that the buoyancy forces are aiding the flow close to the cylinder surface and consequently the velocity gradient increases significantly with the increase of Ri, an effect which is more pronounced at Pr = 1 when the boundary layer is relatively thick.

Representative plots of the streamlines and isotherm contours showed that for a fixed value of the temperature-thinning index b, an increase in power-law index resulted in a slight increase in distance between the streamlines, and between the isothermal lines, in the downstream region. Moreover, for a fixed value of power-law index n, an increase in temperature-thinning index b did not seem to have produced any significant change in the qualitative nature of the streamline and isotherm patterns. Both the aforementioned observations indicate that the effect of temperature thinning index on the streamline and isotherm patterns is quite limited.

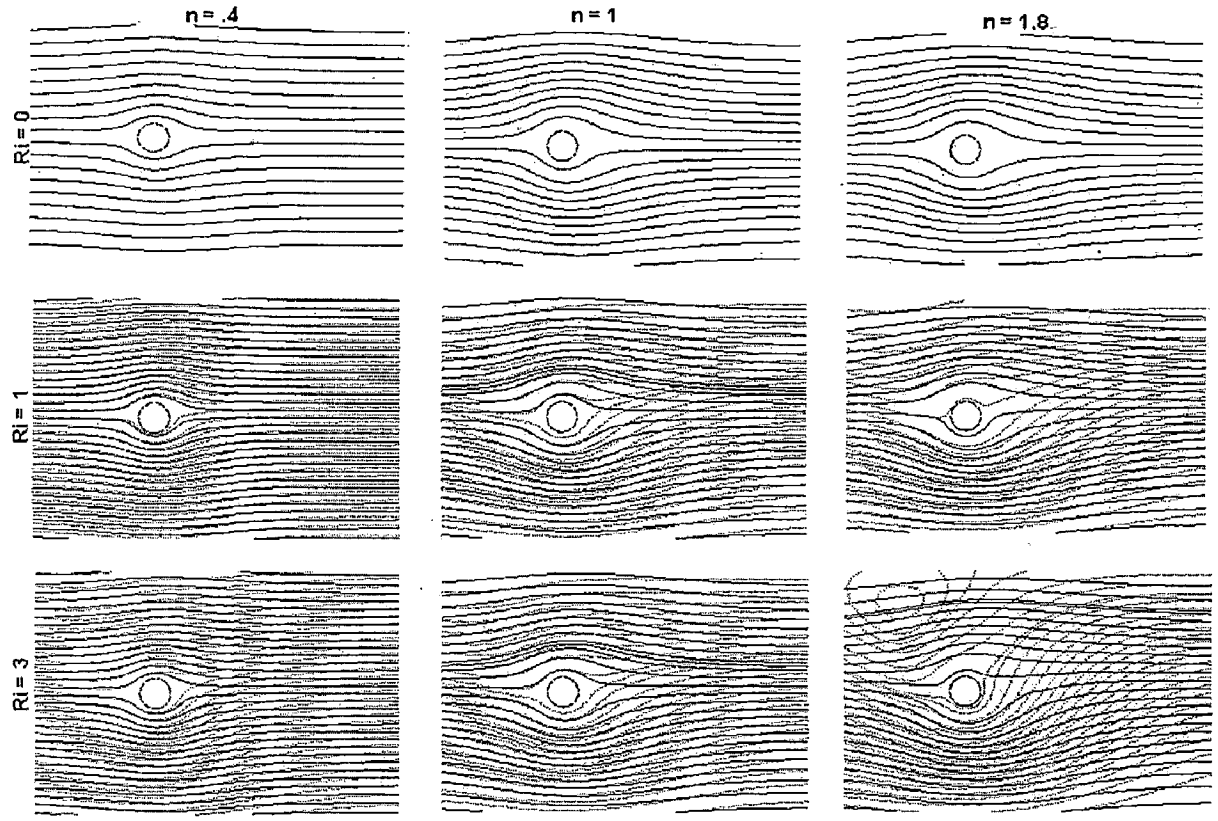

Figure 11 Influence of Richardson numberon the streamline contours for flow at Re = 1 and Pr =1,100 (solid line corresponds to Pr = 100 and dashed line corresponds to Pr = 1, flow direction – left to right)

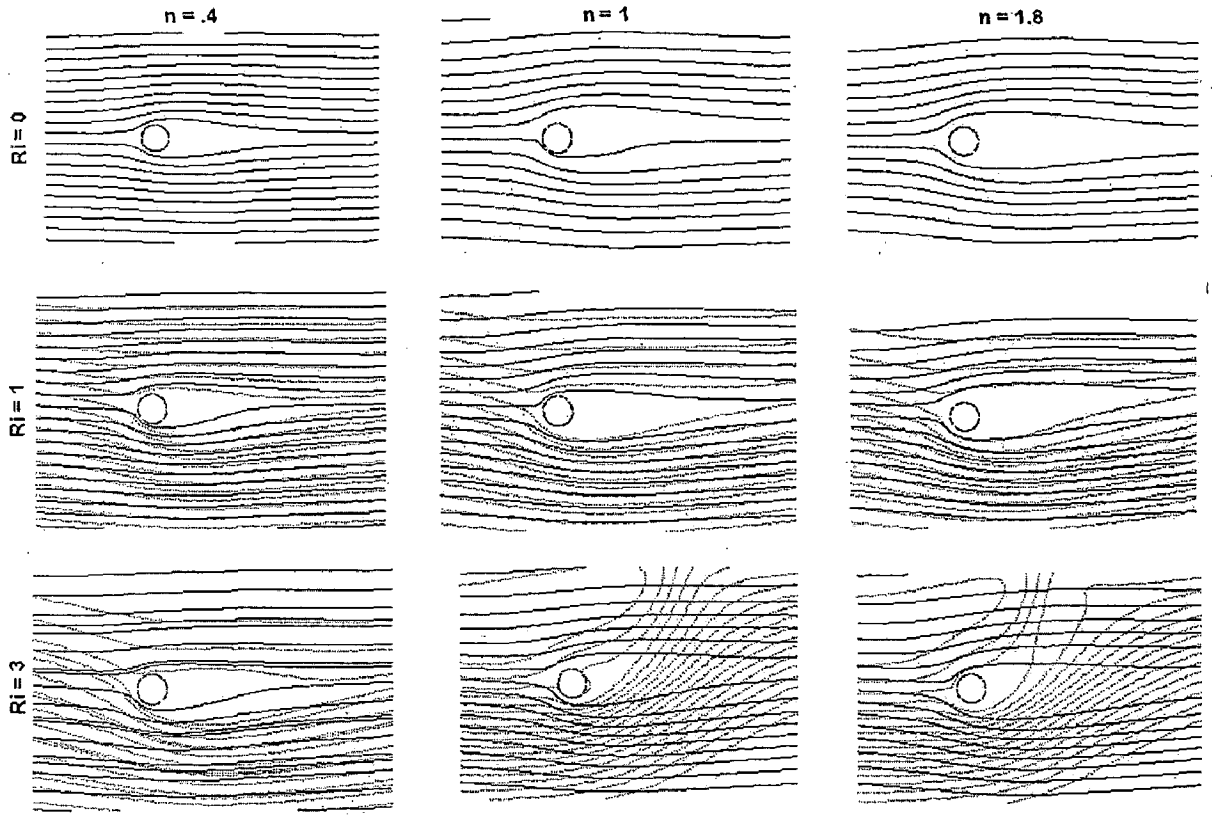

Figure 12 Influence of Richardson numberon the streamline contours for flow at Re = 40 and Pr =1,100 (solid line corresponds to Pr = 100 and dashed line corresponds to Pr = 1, flow direction – left to right)

4.8 Isotherm Patterns

This study also showed asymmetry of the isotherm patterns for mixed convection (Figures 13 and 14) and that such asymmetry exhibited a complex dependence on the Reynolds number (*Re* = 1 and 40) and Prandtl number (*Pr* = 1 and 100), as well as on the power law index (*n* =) 0.4, 1, 1.8). The extent of such symmetry-breaking is characterized by a distortion in the isotherms which increased anticlockwise as mixed convection increased, i.e. with greater *Ri*, and did not occur in the absence of mixed convection, i.e. at *Ri* = 0. This effect becomes less pronounced with the decreasing value of the power law index, an observation that can qualitatively be explained by the fact that the values of effective fluid viscosity decrease with the increasing degree of shear-thinning behavior, which increases the flow rate close to the cylinder surface, consequently

reducing the effect of buoyancy forces on the isotherms. The present study also showed that in the presence of mixed convection (and also in its absence), a decrease in power law index from n = 1.8 to 0.4 resulted in slight overall increase in compactness of the isothermals, which slightly increased the temperature gradient overall. A similar trend was observed as Prandtl number increased from Pr = 1 to 100, although in this case the increase in temperature gradient was much steeper, presumably due to the thinning of the thermal boundary layer. In general, a higher temperature gradient close to the cylinder surface is visible from the isotherm contours. Temperature contours are denser around the front of the cylinder than in its rear, indicating that convective cooling of the cylinder surface is more intense upstream.

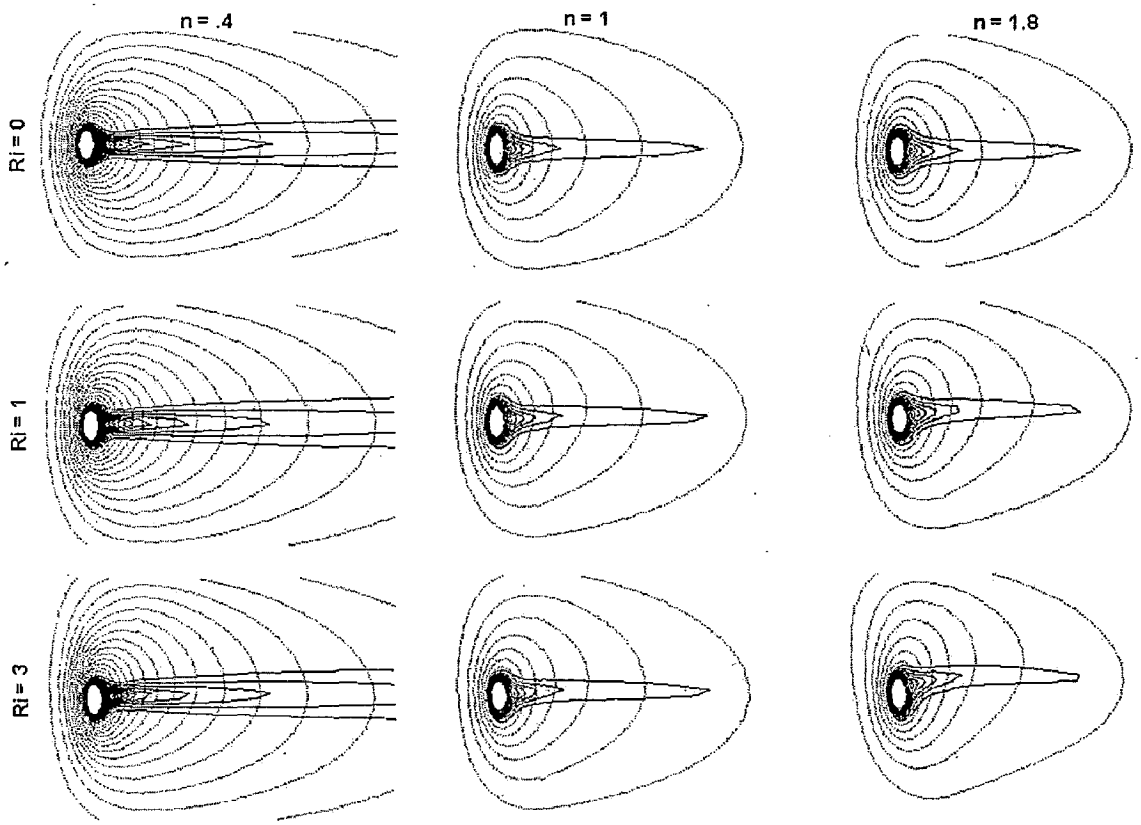

Figure13 Influence of the Richardson number (Ri = 0,1, 3) and Prandtl number (Pr= 1, 100) on the isotherm patterns in the vicinity of an isothermal cylinder for power-law index n = 0.4, 1, 1.8 at a Reynolds number of (Re = 1).

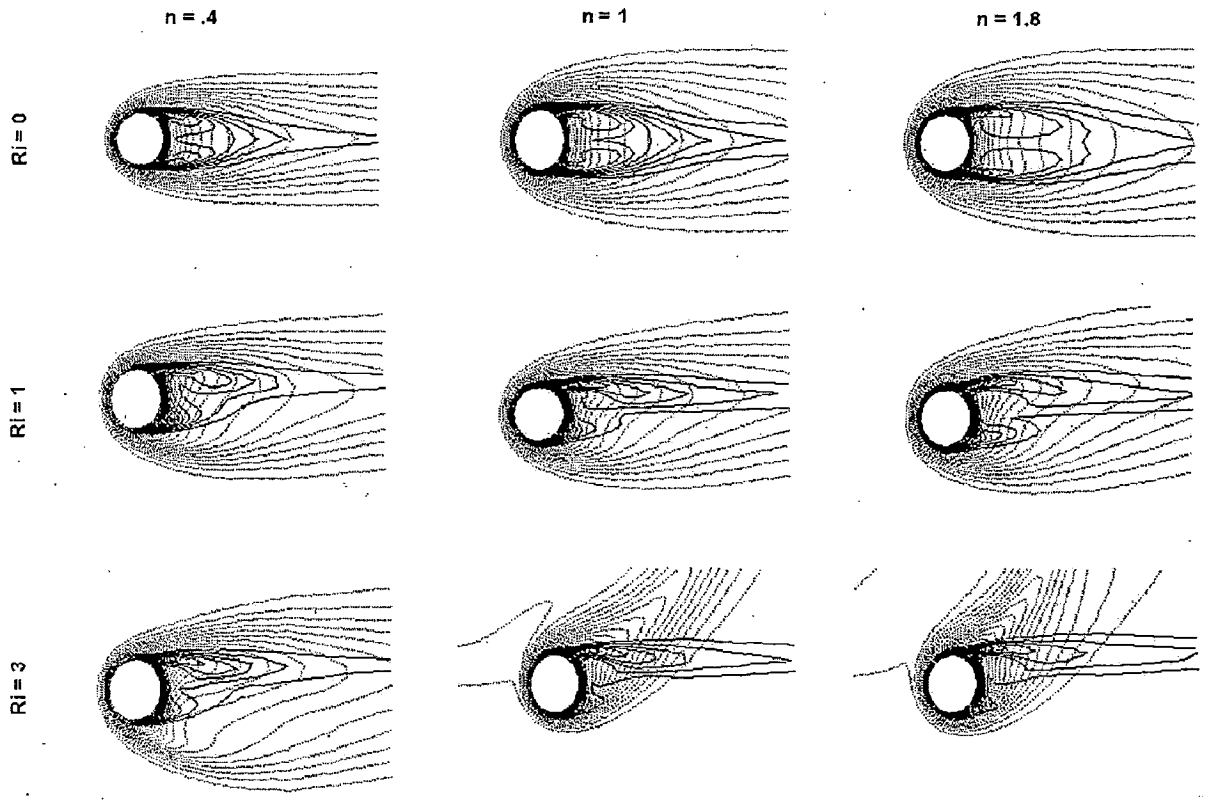

Figure 4 Influence of the Richardson number (Ri = 0,1, 3) and Prandtl number (Pr= 1, 100) on the isotherm patterns in the vicinity of an isothermal cylinder for power-law index n = 0.4, 1, 1.8 at a Reynolds number of (Re = 40).

CHAPTER – 5

CONCLUSIONS AND RECOMMENDATIONS

5.1 Conclusions

In this work, momentum and heat transfer across an unconfined circular cylinder is studied for wide range of parameters: Reynolds number (Re) = 1-40, Prandtl number (Pr) = 1-100, Richardson number (Ri) = 0-3, power law index (n) = 0.4-1.8, temperature thinning index (b) = 0-1. The finite volume method based commercial CFD package FLUENT is used to solve the flow and energy equations. Flow parameters such as total drag coefficient (C_d) and surface averaged Nusselt number (Nu) are obtained and compared with the available values in the literature in order to validate the model.

The hydrodynamic drag force component shows that an increase in Richardson number from Ri = 0 to 3 resulted in increase in values of C_d with Prandtl number 1-100, Reynolds number 1-40 & b = 0-1 irrespective of the fluid behavior index (n). Also on increasing the temperature thinning index from 0 to 1, there was a decrease in the values of drag coefficient.

For fixed values of the parameters (*Ri, Re, Pr*), the average Nusselt number increases as the fluid behavior changes from Newtonian (n = 1) to shear-thinning (n < 1); however, the opposite effect is seen in shear-thickening ($n \geq$ 1) fluids. Also increasing the values of temperature thinning index shows an increase in the values of surface averaged Nusselt number.

Streamline and isotherm contours are also presented in order to describe the flow and temperature field near the cylinder.

5.2 Recommendations for future work

This thesis has contributed to the understanding the effects of fluid flow and heat transfer across a circular cylinder in an unconfined flow.

- Further research along similar lines can help broaden our understanding of the flow around circular and other geometries with extensive ranges of different computational parameters.
- Study can also be extended to different flow regimes eg. Transition or turbulent regimes.
- Temperature variations of other thermo physical can also be incorporated in the models.
- Further 3D simulations can also be performed to comprehend the real life scenarios across a bluff body.

REFERENCES

Bharti, R.P, Chhabra, R.P, Eswaran, V. (2006) Steady flow of power law fluids across a circular cylinder, *The Canadian journal of chemical engineering*,(84).

Bharti, R.P, Chhabra, R.P, Eswaran, V. (2007) Steady forced convection heat transfer from a heated circular cylinder to power-law fluids. *Int. J. of Heat and Mass Transfer* (50):977–990.

Bharti, R.P, Chhabra, R.P, Eswaran, V. (2007) A numerical study of the steady forced convection heat transfer from an unconfined circular cylinder, *Heat Mass Transfer* (43):639-648.

Bharti, R.P, Chhabra, R.P and Eswaran, (2005) Forced Convection Heat Transfer to Non-Newtonian Power-Law Fluids from a Heated Circular Cylinder, New Delhi.

Chhabra, R.P. (1999) Heat and mass transfer in rheologically complex systems. In Advances in the Rheology and Flow of Non-Newtonian Fluids; Siginer, D., De Kee, D., Chhabra, R. P., Eds.; Elsevier: Amsterdan, Chapter 39.

Chhabra, R.P. (2006) Bubbles, Drops and Particles in Non-Newtonian Fluids, second ed.; CRC Press: Boca Raton, FL,

Dhiman, A.K., Anjaiah, N., Chhabra, R.P., Eswaran, V.(2007) Mixed Convection From a Heated Square Cylinder to Newtonian and Power-Law Fluids, *Journal of Fluids Engineering*,(129):506-513.

Fred Stern Fall, (2009) Bluff Body, Intermediate Fluid Mechanics (58:160).

Merkin, J.H., (1976) Mixed convection from a horizontal circular cylinder. *Int.J. Heat Mass Transfer* (20):73-77.

Mohammed, H.A., Salman, Y.K., (2007) Experimental investigation of mixed convection heat transfer for thermally developing flow in a horizontal circular cylinder. *Applied Thermal Engineering* (27):1522–1533.

Patnana, V.K., Bharti, R.P., Chhabra, R.P.,(2010) Two-dimensional unsteady forced convection heat transfer in power-law fluids from a cylinder. Int. J. Heat and Mass Transfer (53):415241.

Soares, A.A, Ferreira, J.M. and Chhabra, R.P. (2005) Flow and Forced Convection Heat Transfer in Cross flow of Non-Newtonian Fluids over a Circular Cylinder. *Ind. Eng. Chem.* Res.(44)5815-5827.

Sivakumar, Bharti, R.P, Chhabra,R.P.(2006) Effect of power law index on critical parameters for power law flow across an unconfined circular cylinder, *Chemical engineering science* (61):6035-6046.

Soares, A.A, Anacleto, J., Caramelo, L., Ferreira, J.M., and Chhabra,R.P.(2009) Mixed Convection From a Circular Cylinder to Power Law Fluids. *Ind. Eng. Chem.* Res.48, 8219-8231.

Srinivas, A.T, Bharti, R.P. and Chhabra, R.P. (2009) Mixed Convection Heat Transfer from a Cylinder in Power-Law Fluids: Effect of Aiding Buoyancy. *Ind. Eng. Chem.* Res. 48:9735–9754.